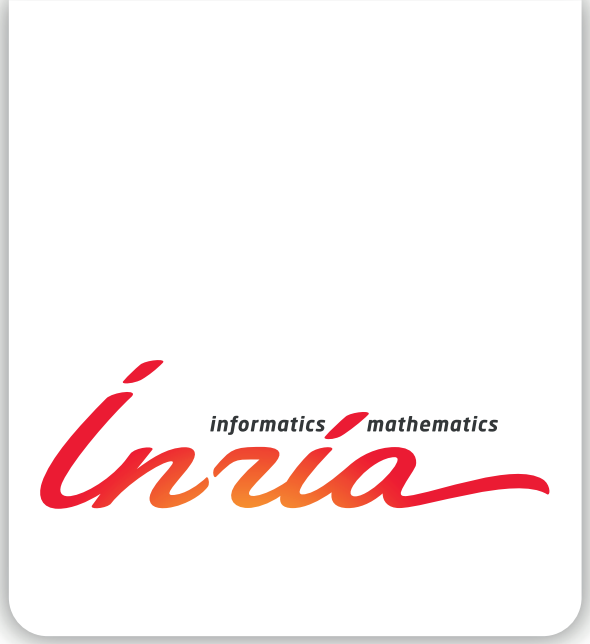

Description of turbulent dynamics in the interstellar medium:

multifractal/microcanonical analysis

H. Yahia, N. Schneider, S. Bontemps, L. Bonne, G. Attuel, S. Dib, V. Ossenkopf, A. Turiel, A. Zebadua, D. Elia, S. Kumar Maji, F. G. Schmitt, J.-F. Robitaille

DFG-ANR Genesis Project

sftools-bigdata

Oct. 27th to 30th 2020

1
New multifractal tools
well suited for astronomy

Overview

Evaluate the multifractal characteristics (e.g. singularity spectrum) in one spatial observation map.

Overview

Evaluate the multifractal characteristics (e.g. singularity spectrum) in one spatial observation map.

Approach based on concepts from predictability in complex systems.

Overview

Evaluate the multifractal characteristics (e.g. singularity spectrum) in one spatial observation map.

Approach based on concepts from predictability in complex systems.

Easy check of scale invariance.

Overview

Evaluate the multifractal characteristics (e.g. singularity spectrum) in one spatial observation map.

Approach based on concepts from predictability in complex systems.

Easy check of scale invariance.

An observation map must be correctly filtered for proper noise elimination. We introduce a novel sparse filtering approach.

Overview

Evaluate the multifractal characteristics (e.g. singularity spectrum) in one spatial observation map.

Approach based on concepts from predictability in complex systems.

Easy check of scale invariance.

An observation map must be correctly filtered for proper noise elimination. We introduce a novel sparse filtering approach.

We apply the tools to the Musca cloud: we observe asymmetries (deviation from log-normality) in certain regions of a cloud.

Turbulence and the ISM

The turbulent nature of the ISM is well established by the extremely high values of Reynolds number.

[Elmegreen & Scalo 2004; Kowal et al. 2007; Burkhart et al. 2009a,b; Schneider et al. 2011; Seifried & Walch 2015; Kritsuk et al. 2017; Mocz et al. 2017; Elia et al. 2018; Lee & Lee 2019]

[Scalo 1987; Green 1993; Stutzki et al. 1998; Robitaille et al. 2020]

Turbulence and the ISM

The turbulent nature of the ISM is well established by the extremely high values of Reynolds number.

Galactic studies of emission lines of atomic hydrogen or molecules: Fourier power spectrum well fitted by a power law $\rightarrow$ scaling properties.

[Elmegreen & Scalo 2004; Kowal et al. 2007; Burkhart et al. 2009a,b; Schneider et al. 2011; Seifried & Walch 2015; Kritsuk et al. 2017; Mocz et al. 2017; Elia et al. 2018; Lee & Lee 2019]

[Scalo 1987; Green 1993; Stutzki et al. 1998; Robitaille et al. 2020]

Turbulence and the ISM

The turbulent nature of the ISM is well established by the extremely high values of Reynolds number.

Galactic studies of emission lines of atomic hydrogen or molecules: Fourier power spectrum well fitted by a power law $\rightarrow$ scaling properties.

Δ-variance, scaling of correlation functions $\rightarrow$ scaling properties.

[Elmegreen & Scalo 2004; Kowal et al. 2007; Burkhart et al. 2009a,b; Schneider et al. 2011; Seifried & Walch 2015; Kritsuk et al. 2017; Mocz et al. 2017; Elia et al. 2018; Lee & Lee 2019]

[Scalo 1987; Green 1993; Stutzki et al. 1998; Robitaille et al. 2020]

Kolmogorov scaling

Velocity field $\mathbf{v}(\mathbf{x})$, $\mathbf{u}$ specific fixed direction defined by a unitary vector.

[Frisch 1995]

Kolmogorov scaling

Velocity field $\mathbf{v}(\mathbf{x})$, $\mathbf{u}$ specific fixed direction defined by a unitary vector.

Inside the inertial range $[\mathbf{r}_1, \mathbf{r}_2]$, scaling of the moments:

$$\langle |(\mathbf{v}(\mathbf{x} + \mathbf{r}\mathbf{u}) - \mathbf{v}(\mathbf{x})) \cdot \mathbf{u}|^q \rangle \sim \mathbf{r}^{\xi(q)}. \quad (1)$$

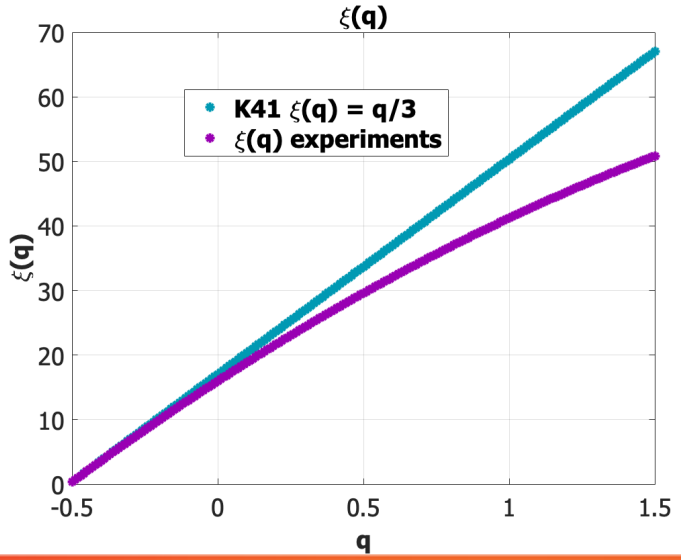

[Frisch 1995]

Multifractal models of intermittency

Let us denote by $\mathcal{F}_{\mathbf{h}}$ the set of points $\mathbf{x}$ whose velocity increments, measured in the unitary direction $\mathbf{u}$ as before, behave as $\mathbf{r}^{\mathbf{h}}$ for a certain $\mathbf{h}$ i.e.

$$\mathcal{F}_{\mathbf{h}} = \{\mathbf{x} \text{ s.t. } |(\mathbf{v}(\mathbf{x}+\mathbf{ru}) - \mathbf{v}(\mathbf{x})) \cdot \mathbf{u}| \sim \mathbf{r}^{\mathbf{h}} \text{ when } \mathbf{r} \to 0\}.$$

Multifractal models of intermittency

Let us denote by $\mathcal{F}_{\mathbf{h}}$ the set of points $\mathbf{x}$ whose velocity increments, measured in the unitary direction $\mathbf{u}$ as before, behave as $\mathbf{r}^{\mathbf{h}}$ for a certain $\mathbf{h}$ i.e.

$$\mathcal{F}_{\mathbf{h}} = \{\mathbf{x} \text{ s.t. } |(\mathbf{v}(\mathbf{x}+\mathbf{ru}) - \mathbf{v}(\mathbf{x})) \cdot \mathbf{u}| \sim \mathbf{r}^{\mathbf{h}} \text{ when } \mathbf{r} \to 0\}.$$

$$D(\mathbf{h}) = \dim_H(\mathcal{F}_{\mathbf{h}}).$$

Multifractal models of intermittency

Let us denote by $\mathcal{F}_{\mathbf{h}}$ the set of points $\mathbf{x}$ whose velocity increments, measured in the unitary direction $\mathbf{u}$ as before, behave as $\mathbf{r}^{\mathbf{h}}$ for a certain $\mathbf{h}$ i.e.

$$\mathcal{F}_{\mathbf{h}} = \{\mathbf{x} \text{ s.t. } |(\mathbf{v}(\mathbf{x}+\mathbf{ru}) - \mathbf{v}(\mathbf{x})) \cdot \mathbf{u}| \sim \mathbf{r}^{\mathbf{h}} \text{ when } \mathbf{r} \to 0\}. \quad (2)$$

$$D(\mathbf{h}) = \dim_H(\mathcal{F}_{\mathbf{h}}).$$

Link between geometrical complexity and statistical behavior :

$$\xi(q) = \inf_{\mathbf{h}>0}(q\mathbf{h} + d - D(\mathbf{h})),$$

i.e. $\xi(q)$ appears as a Legendre transform. The mapping $\mathbf{h} \mapsto D(\mathbf{h})$ is called the **singularity spectrum** of the velocity field.

Singularity spectrum

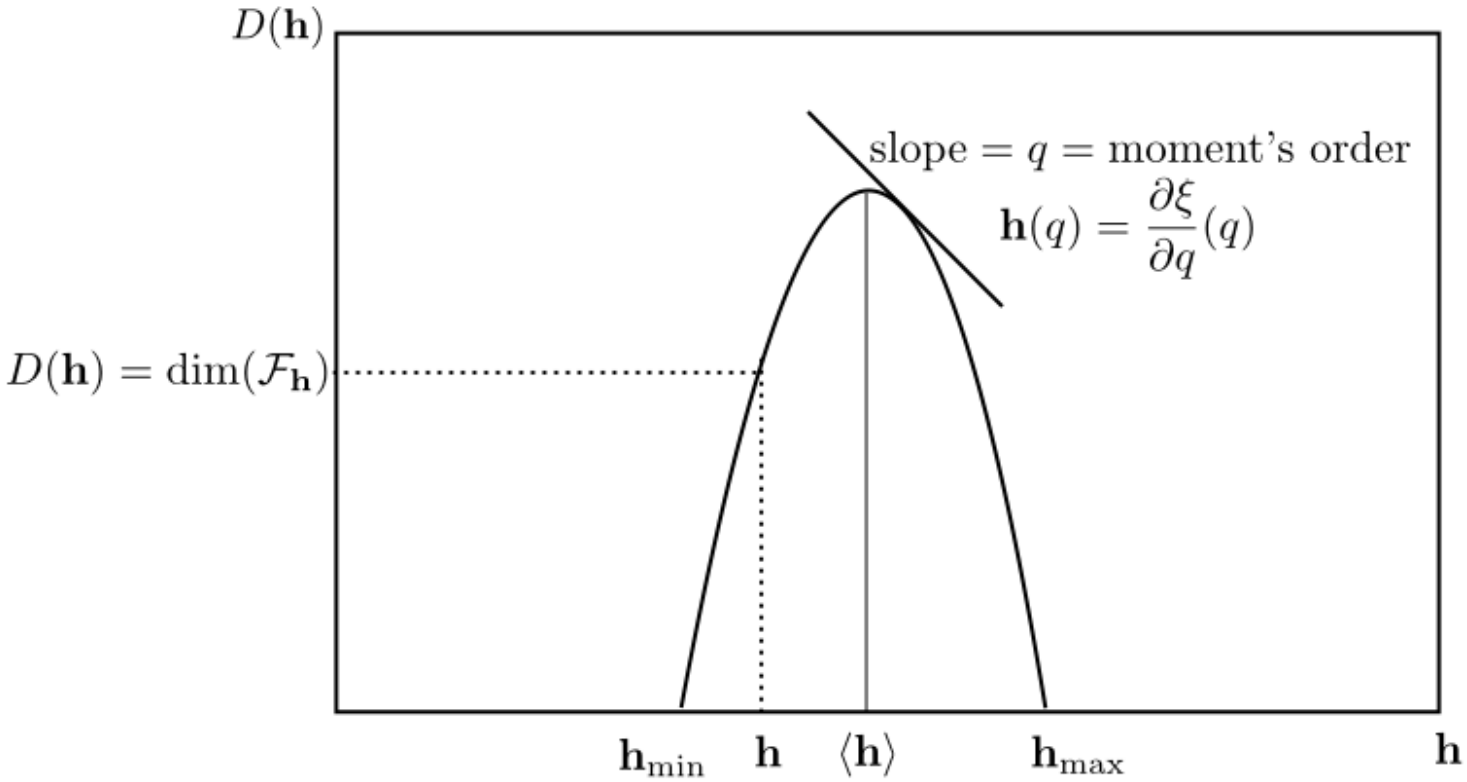

General form of the singularity spectrum $D(\mathbf{h})$, Legendre transform of $\xi(q)$.

2
Musca Herschel observation map

Herschel flux density map

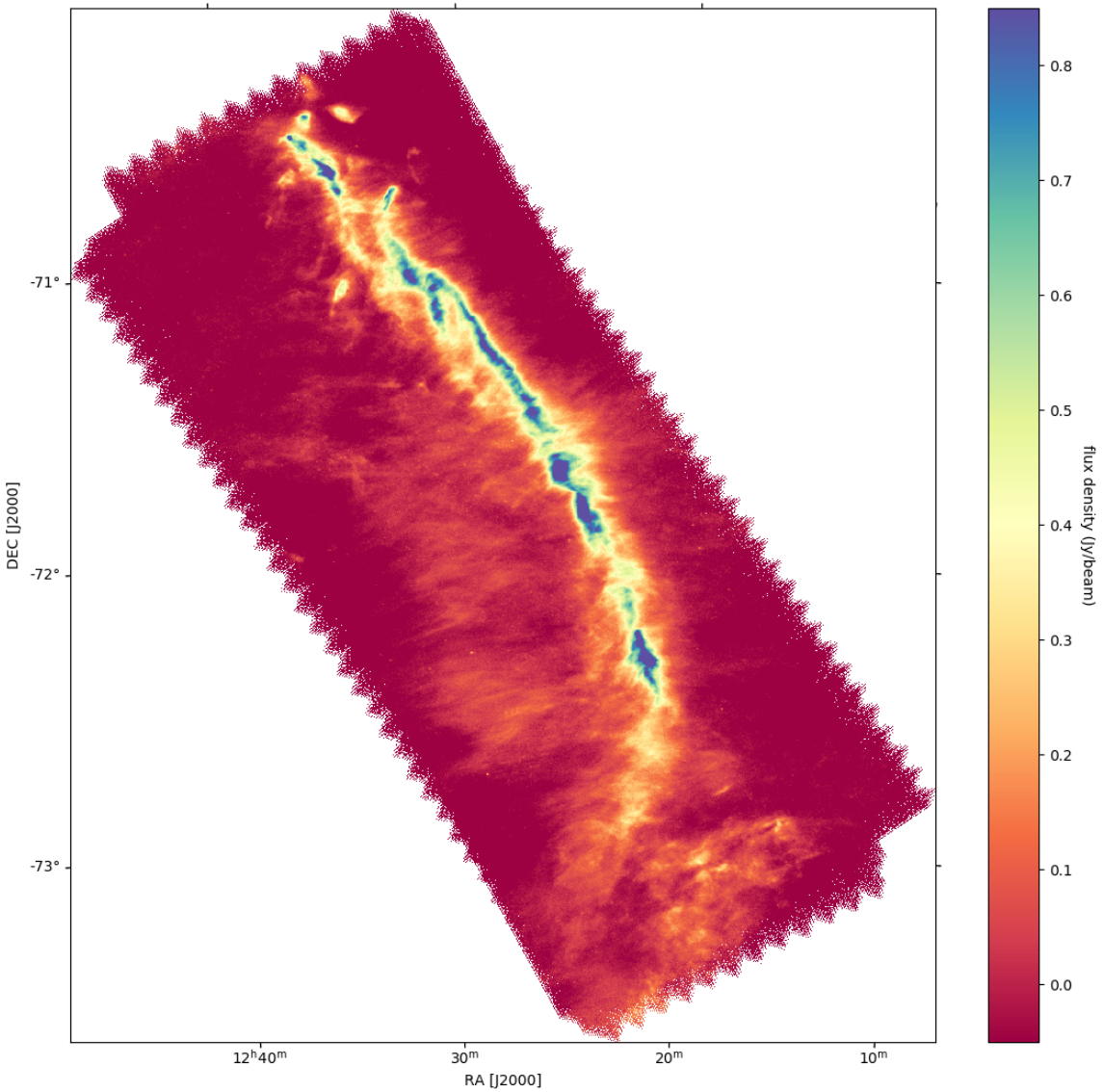

Musca flux density map from *Herschel* at 250 μm.

[Cox2016; Kainulainen2016;]

[Gaia collaboration 2018; Bonne2020a,b]

3
Signal analysis with multifractal tools:
existing methods

Canonical ensemble

Wavelet Transform Maximum Modulus (WTMM).

Cumulant analysis.

Wavelet leaders.

Multifractal detrended fluctuation analysis.

[Arneodo et al. 1995; Kantelhardt et al. 2002; Venugopal et al. 2006; Serrano & Figliola 2009]

Canonical ensemble

These methods are statistical. They suppose the availability of grand ensembles of realizations of a same map.

[Arneodo et al. 1995; Kantelhardt et al. 2002; Venugopal et al. 2006; Serrano & Figliola 2009]

Canonical ensemble

These methods are statistical. They suppose the availability of grand ensembles of realizations of a same map.

The signal is wavelet projected and partition functions are defined depending on scale.

[Arneodo et al. 1995; Kantelhardt et al. 2002; Venugopal et al. 2006; Serrano & Figliola 2009]

Canonical ensemble

These methods are statistical. They suppose the availability of grand ensembles of realizations of a same map.

The signal is wavelet projected and partition functions are defined depending on scale.

Computation of the singularity spectrum through log-regression.

[Arneodo et al. 1995; Kantelhardt et al. 2002; Venugopal et al. 2006; Serrano & Figliola 2009]

Microcanonical

Counting-box methods, histogram method, gradient-modulus wavelet projection.

[Arneodo et al. 1995; Venugopal et al. 2006]

Microcanonical

Counting-box methods, histogram method, gradient-modulus wavelet projection.

Devised early but abandoned in the signal processing community because of low accuracy and precision.

[Arneodo et al. 1995; Venugopal et al. 2006]

Microcanonical

Counting-box methods, histogram method, gradient-modulus wavelet projection.

Devised early but abandoned in the signal processing community because of low accuracy and precision.

In this context, the singularity spectrum $\mathbf{h} \mapsto D(\mathbf{h})$ is the entropy per unit volume, so that the computation of the singularity spectrum is equivalent to the computation of the entropy per internal energy in a large multi-body system.

[Arneodo et al. 1995; Venugopal et al. 2006]

Microcanonical

Counting-box methods, histogram method, gradient-modulus wavelet projection.

Devised early but abandoned in the signal processing community because of low accuracy and precision.

In this context, the singularity spectrum $\mathbf{h} \mapsto D(\mathbf{h})$ is the entropy per unit volume, so that the computation of the singularity spectrum is equivalent to the computation of the entropy per internal energy in a large multi-body system.

Singularity exponents are evaluated pointwise:

$$\mathbf{h}(\mathbf{x}) = \lim_{\mathbf{r} \to 0} \frac{\log \mu(\mathcal{B}(\mathbf{x}, \mathbf{r}))}{\log(\mathbf{r})}$$

[Arneodo et al. 1995; Venugopal et al. 2006]

Microcanonical & predictability

New approach based on predictability in complex systems allows an efficient computation of $\mathbf{h}(\mathbf{x})$ and the singularity spectrum.

[Turiel et a. 2008]

Microcanonical & predictability

New approach based on predictability in complex systems allows an efficient computation of $\mathbf{h}(\mathbf{x})$ and the singularity spectrum.

Given an observational map $s(\mathbf{x})$, a subset $\mathcal{F}$ is said to reconstruct the signal s if we have

$$\nabla s(\mathbf{x}) = \mathcal{G}\left(\nabla_{\mathcal{F}} s(\mathbf{x})\right)$$

[Turiel et a. 2008]

Microcanonical & predictability

New approach based on predictability in complex systems allows an efficient computation of $\mathbf{h}(\mathbf{x})$ and the singularity spectrum.

Given an observational map $s(\mathbf{x})$, a subset $\mathcal{F}$ is said to reconstruct the signal s if we have

$$\nabla s(\mathbf{x}) = \mathcal{G}\left(\nabla_{\mathcal{F}} s(\mathbf{x})\right)$$

One can show that this implies

$$\mathrm{div}\left(\nabla_{\mathcal{F}^{\mathsf{C}}} s\right) = 0.$$

with $\mathcal{F}^{\mathsf{C}}$: complementary set of $\mathcal{F} \rightarrow$ the decision $\mathbf{x} \in \mathcal{F}$ **can be done locally**.

[Turiel et a. 2008]

Microcanonical & predictability

The set of most unpredictable points $\mathcal{F}_\infty$ is the one which gives a perfect reconstruction; this set is identical to the set of points which have the lowest singularity exponents in the signal i.e.
$\mathcal{F}_\infty = \mathcal{F}_{\mathbf{h}_\infty} = \{\mathbf{x} \mid \mathbf{h}(\mathbf{x}) = \mathbf{h}_\infty\}$ with $\mathbf{h}_\infty$ being the minimum of the singularity exponents.

[Turiel et a. 2008]

Microcanonical & predictability

The set of most unpredictable points $\mathcal{F}_\infty$ is the one which gives a perfect reconstruction; this set is identical to the set of points which have the lowest singularity exponents in the signal i.e.
$\mathcal{F}_\infty = \mathcal{F}_{\mathbf{h}_\infty} = \{\mathbf{x} \mid \mathbf{h}(\mathbf{x}) = \mathbf{h}_\infty\}$ with $\mathbf{h}_\infty$ being the minimum of the singularity exponents.

Consequence: **the determination of the singularity exponents can be done locally by use of a correlation measure**:

[Turiel et a. 2008]

Microcanonical & predictability

The set of most unpredictable points $\mathcal{F}_\infty$ is the one which gives a perfect reconstruction; this set is identical to the set of points which have the lowest singularity exponents in the signal i.e.
$\mathcal{F}_\infty = \mathcal{F}_{\mathbf{h}_\infty} = \{\mathbf{x} \mid \mathbf{h}(\mathbf{x}) = \mathbf{h}_\infty\}$ with $\mathbf{h}_\infty$ being the minimum of the singularity exponents.

Consequence: **the determination of the singularity exponents can be done locally by use of a correlation measure**:

$$\mathbf{h}(\mathbf{x}) = \frac{\log(\mathcal{H}(\mu_n, \mathbf{x}, \mathbf{r}_0))/\langle \mathcal{H}(\mu_n, \mathbf{x}, \mathbf{r}_0)\rangle}{\log \mathbf{r}_0}$$

$\rightarrow$ the values of the singularity exponents are computed at the lowest scale $\mathbf{r}_0 = 2^{-n}$ of the acquisition signal instead of log-regression through scales.

[Turiel et a. 2008]

Singularity spectrum

To count the sites $\mathbf{x}$ with same scaling behavior, one introduces the density of the exponents at resolution $\frac{1}{2^n}$

$$\rho_n(\mathbf{h}) = \sum_{\mathbf{x}\in\Omega_n} \delta\left(\frac{\log \mu(\mathcal{B}(\mathbf{x}, 2^{1-n}))}{\log 2^n} - \mathbf{h}\right). \tag{3}$$

[Fyodorov 2010, 2012]

Singularity spectrum

To count the sites $\mathbf{x}$ with same scaling behavior, one introduces the density of the exponents at resolution $\dfrac{1}{2^n}$

$$\rho_n(\mathbf{h}) = \sum_{\mathbf{x}\in\Omega_n} \delta\left(\frac{\log \mu(\mathcal{B}(\mathbf{x}, 2^{1-n}))}{\log 2^n} - \mathbf{h}\right). \tag{4}$$

In the limit $n \to +\infty$ one has

$$\rho_n(\mathbf{h}) \sim c_n(\mathbf{h}) \sqrt{n \log 2}\, n^{\log(2) D(\mathbf{h})}$$

where the mapping $\mathbf{h} \mapsto D(\mathbf{h})$ is the singularity spectrum

[Fyodorov 2010, 2012]

Singularity spectrum

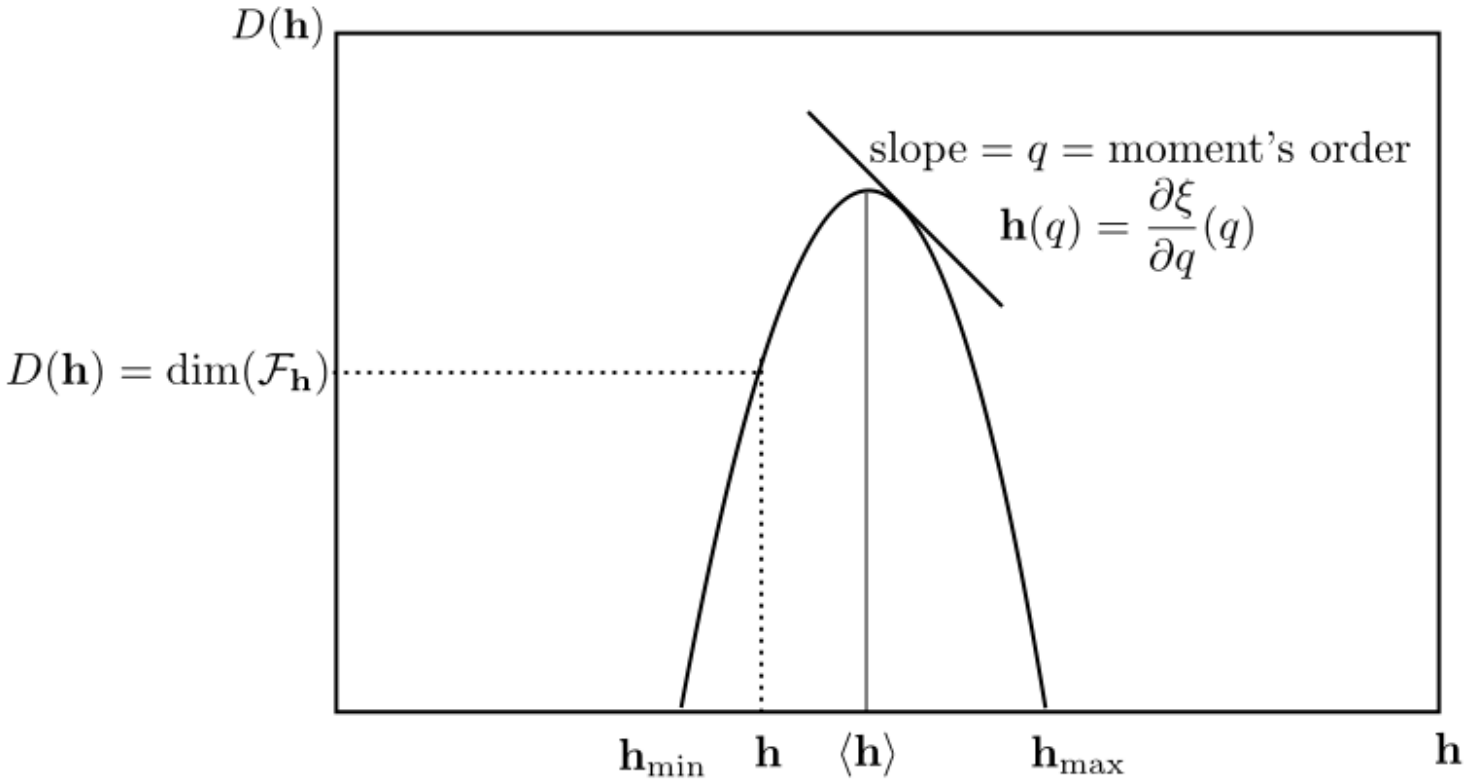

General form of the singularity spectrum $D(\mathbf{h})$, Legendre transform of $\xi(q)$.

E.g. : Herschel flux density map

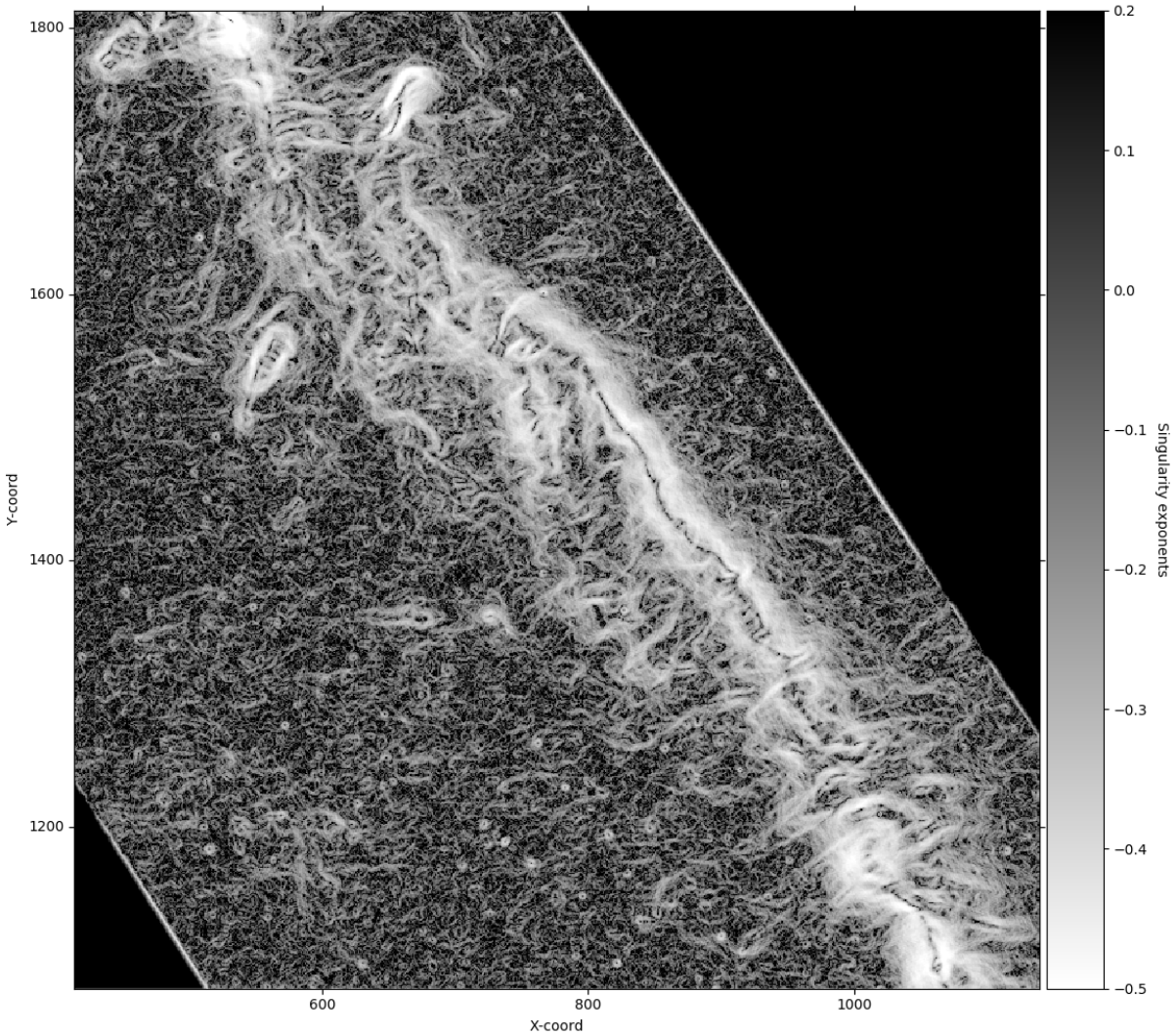

Map of the singularity exponents computed on filtered Musca 250 μm data.

4
Singularity exponents, singularity spectrum

Necessity of sparse filtering an observation map

Noise and filaments

The Musca *Herschel* 250 μm flux map contains point-like sources, which are mostly galaxies, and the cosmic infrared background (CIB) and the cosmic microwave background which have isotropic low amplitude values very close to those of low scale filamentary structures

[Padoan2001a; Robitaille2019]

Noise and filaments

The Musca *Herschel* 250 μm flux map contains point-like sources, which are mostly galaxies, and the cosmic infrared background (CIB) and the cosmic microwave background which have isotropic low amplitude values very close to those of low scale filamentary structures

Filamentary structures are faded out by the noise.

[Padoan2001a; Robitaille2019]

Sparse filtering

The L^1 norm favours sparsity:

$$\underset{s_f}{\text{argmin}} \quad \|s - s_f\|_1 + \lambda \|\nabla s_f\|_1$$

[Candes2008]

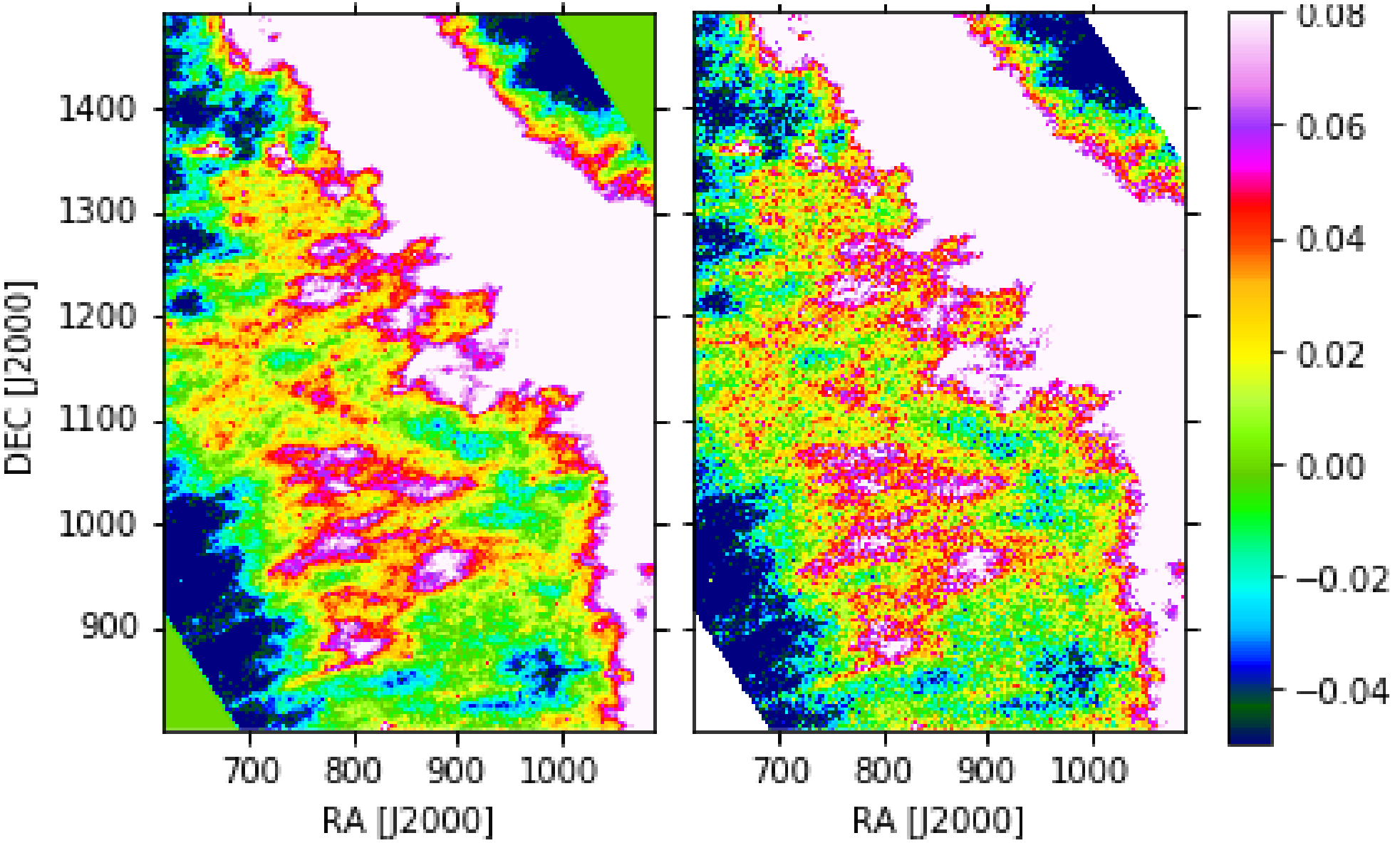
DEC [J2000]
1400
1300
1200
1100
1000
900
700
800
900
1000
RA [J2000]
700
800
900
1000
RA [J2000]
0.08
0.06
0.04
0.02
0.00
−0.02
−0.04

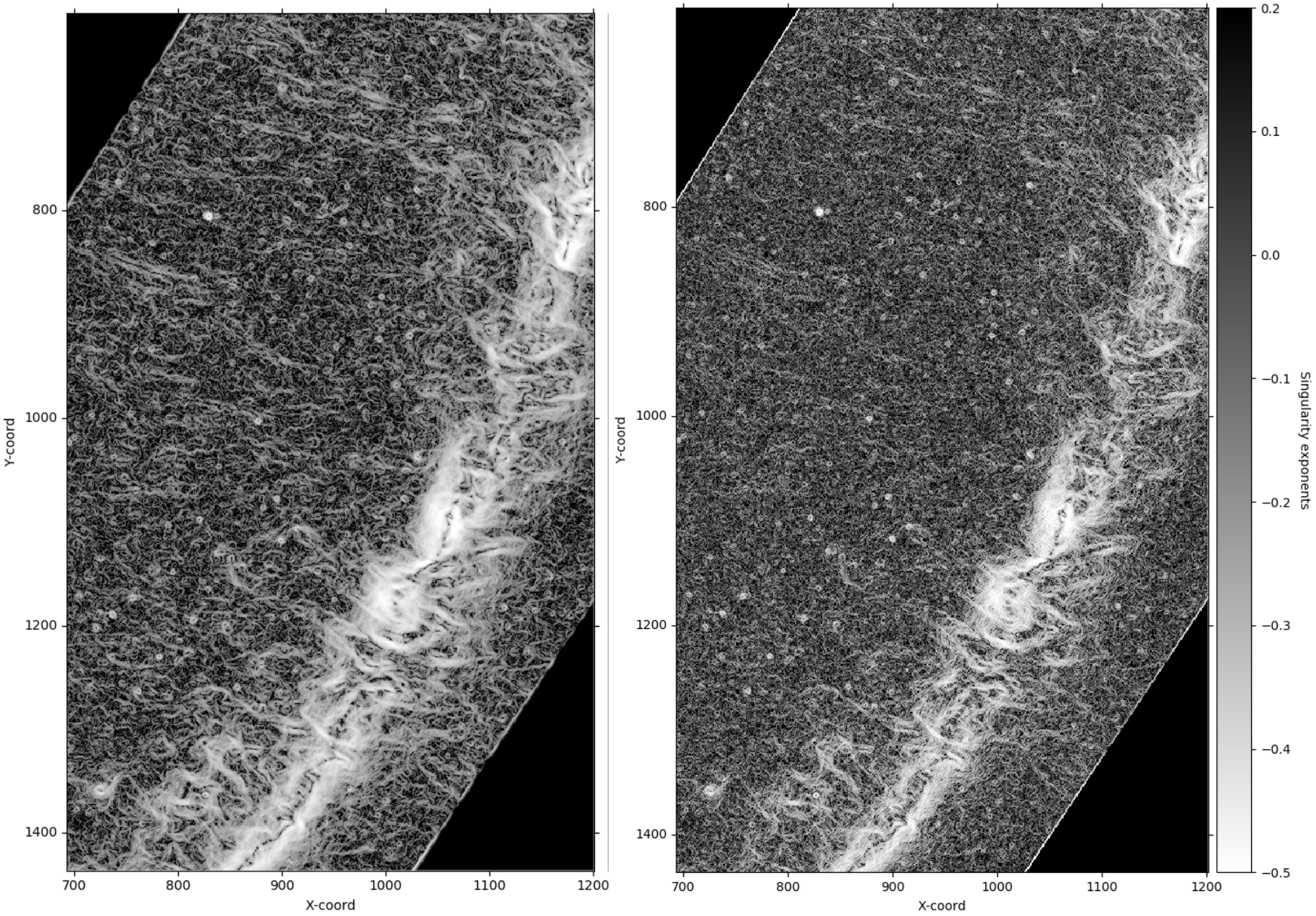
Y-coord
800
1000
1200
1400
700
800
900
1000
1100
1200
X-coord
Y-coord
800
1000
1200
1400
700
800
900
1000
1100
1200
X-coord
0.2
0.1
0.0
−0.1
−0.2
−0.3
−0.4
−0.5
Singularity exponents

Musca (part)

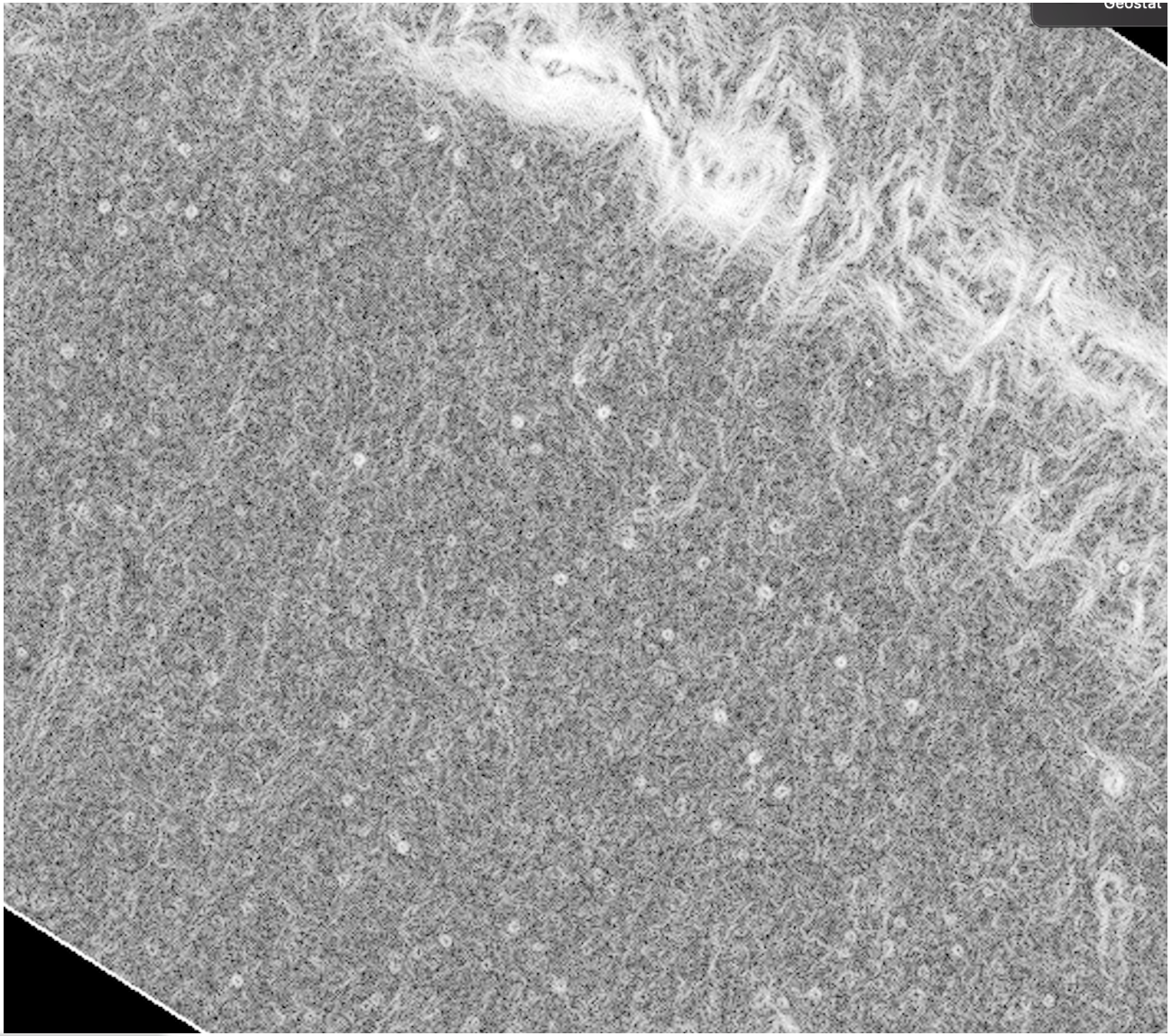

Musca (part)

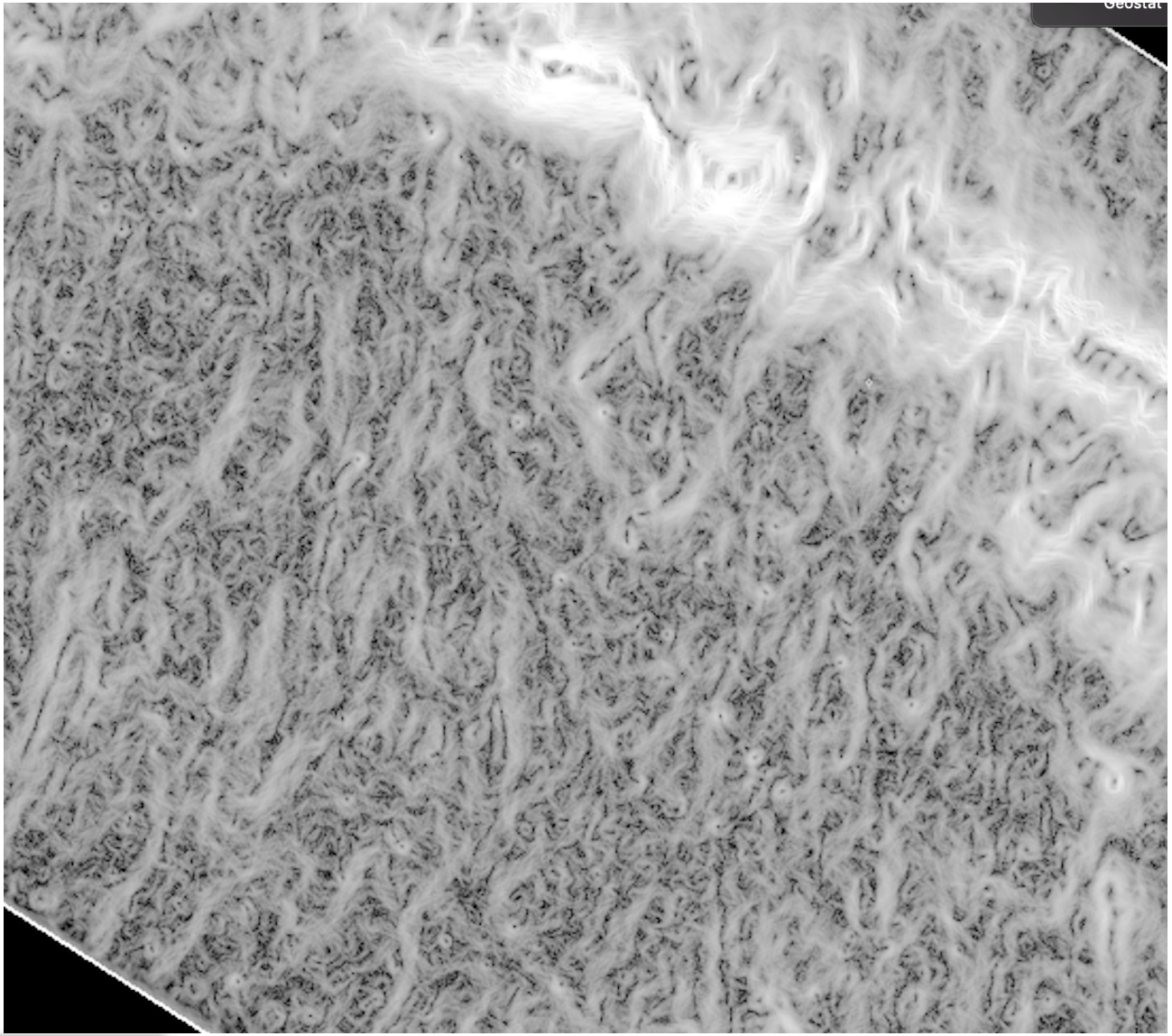

Draco (part)

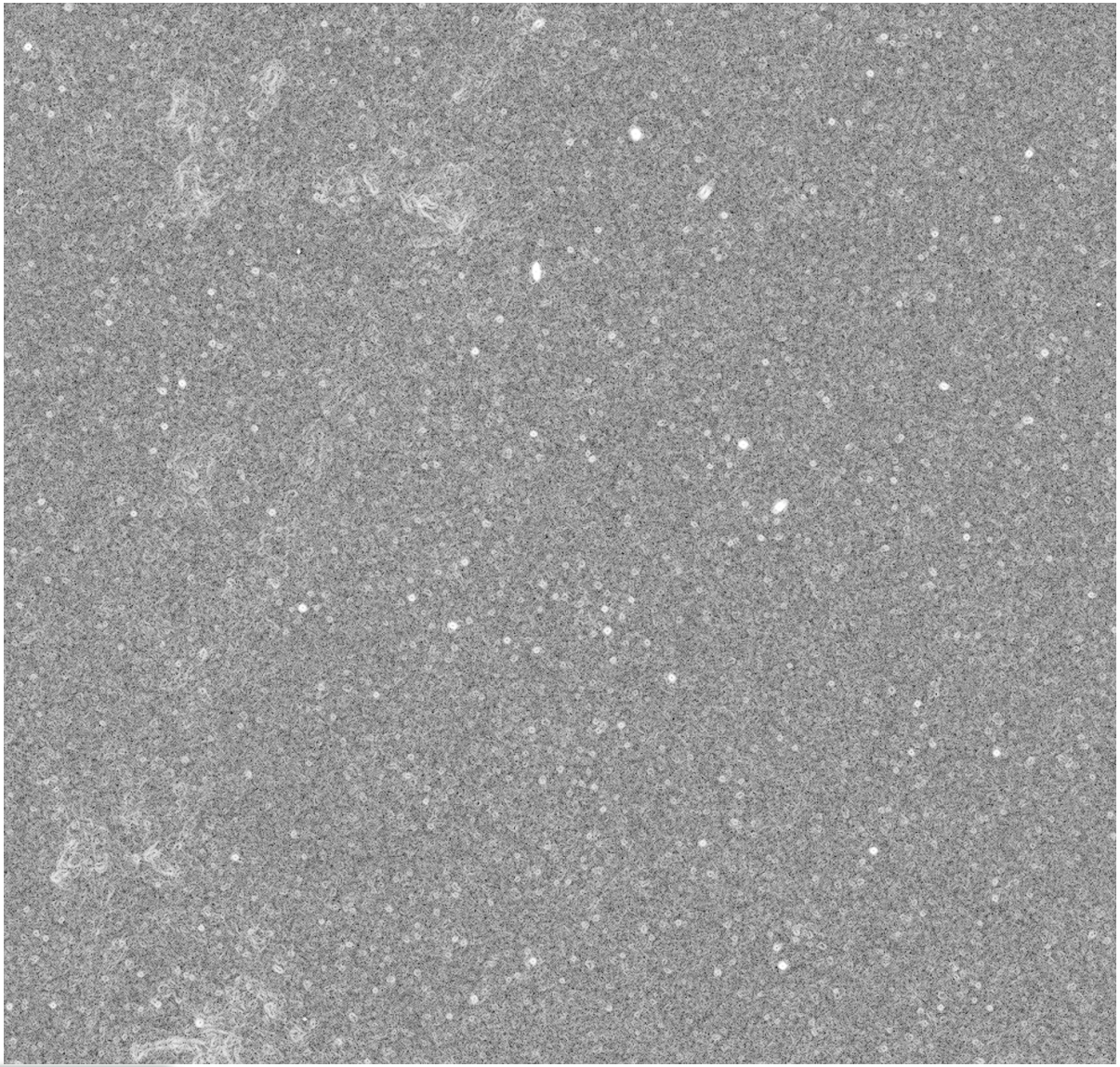

Draco (part)

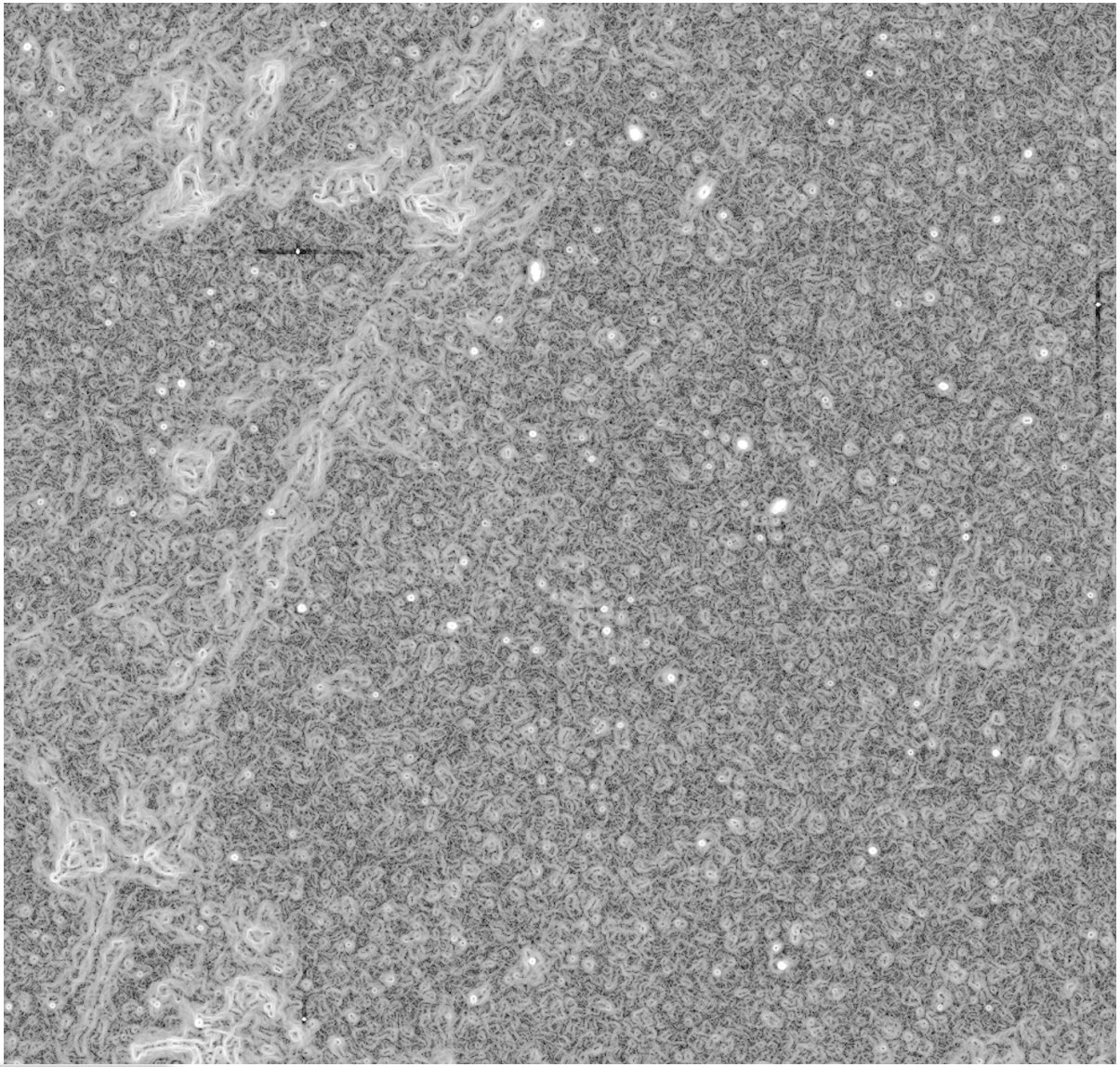

Spider

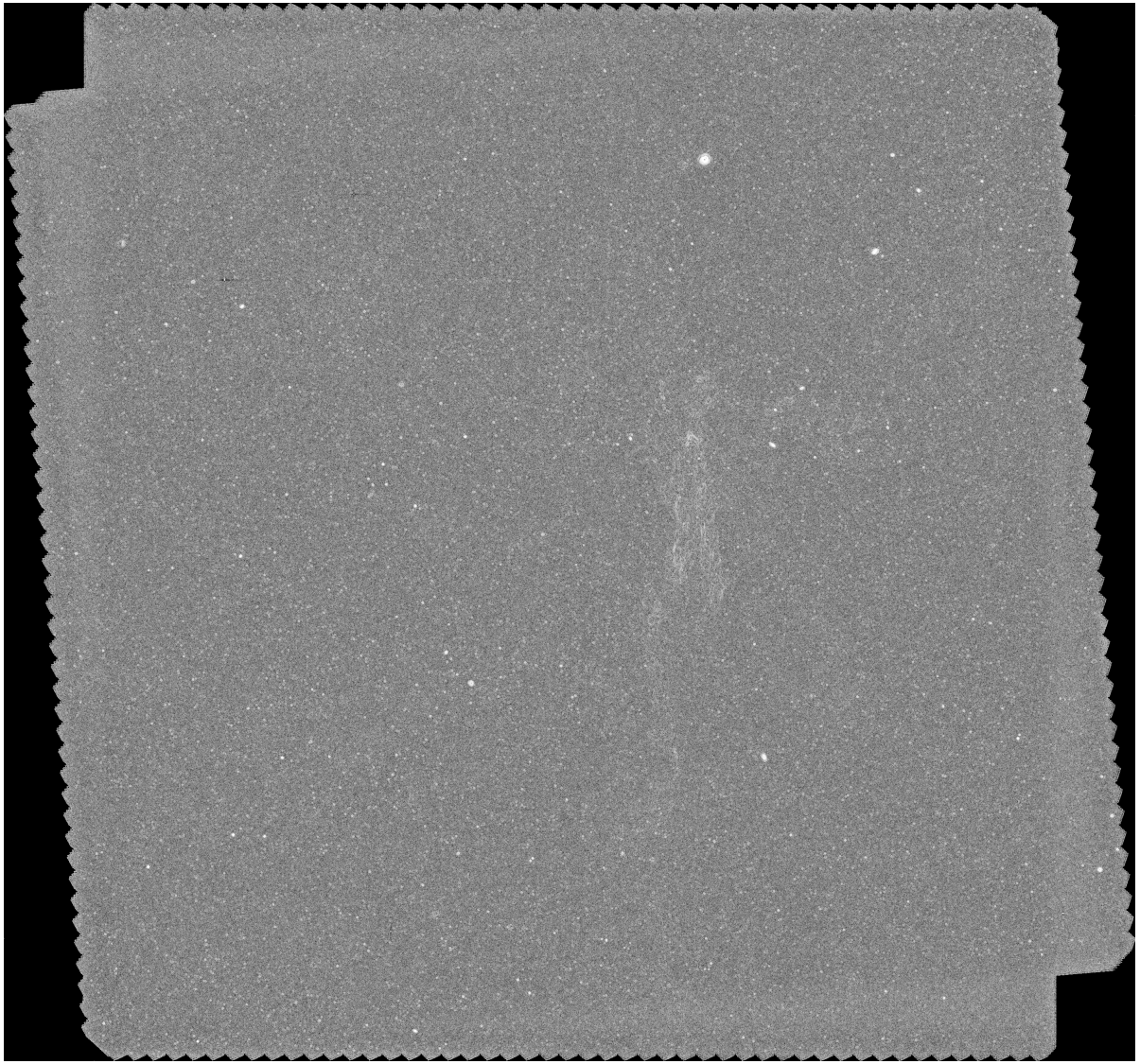

Spider

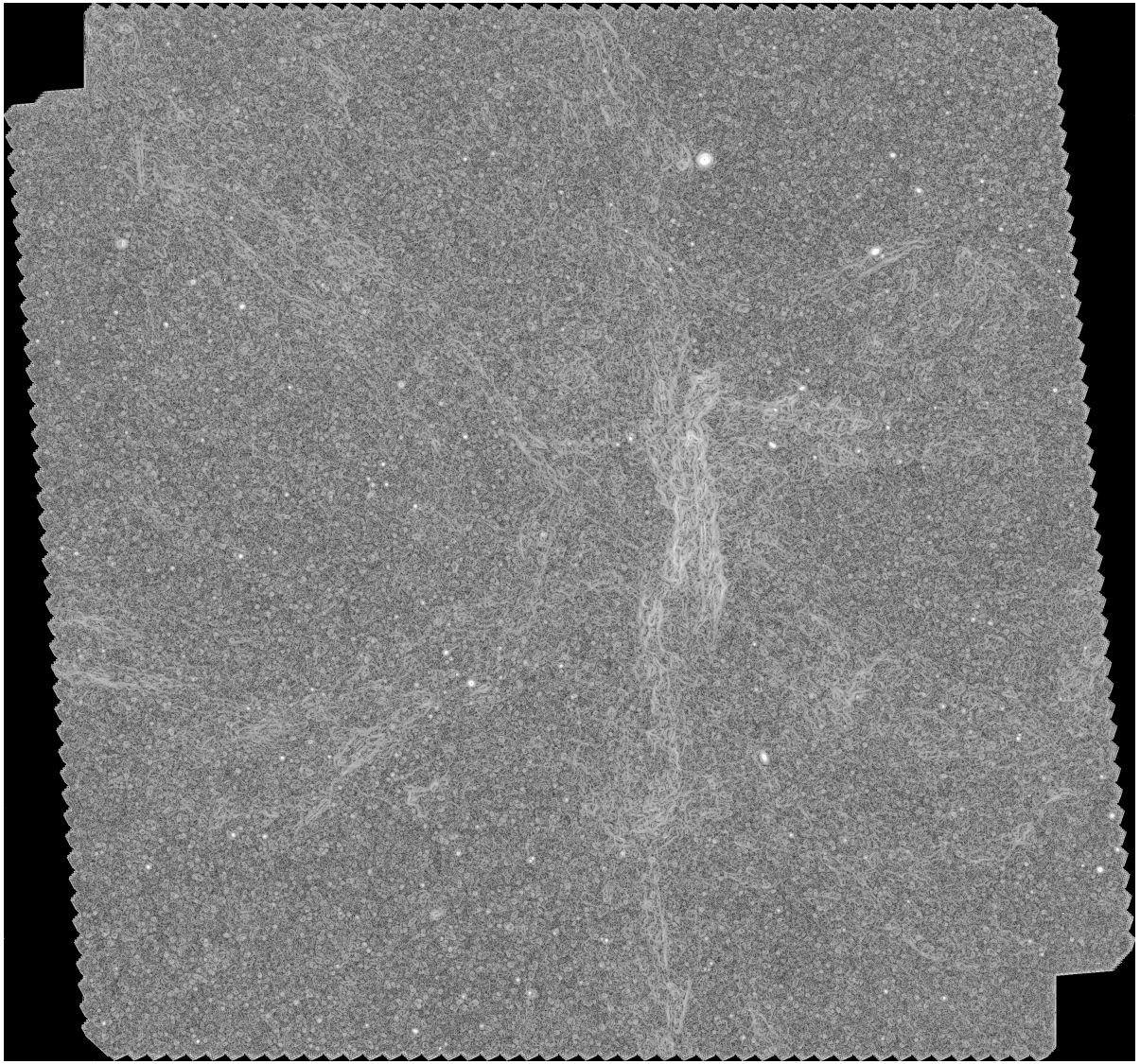

CIB "gaussianizes" a singularity spectrum

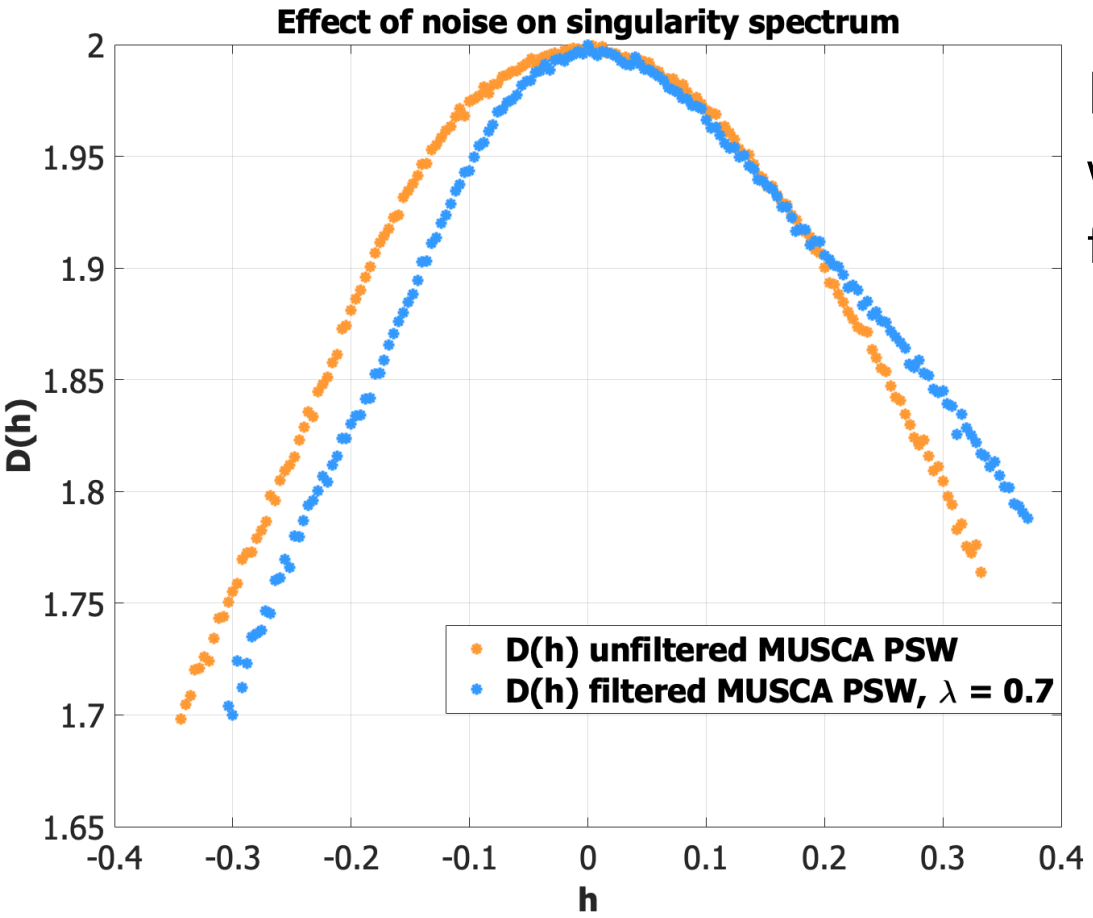

Musca 250 μm *Herschel* map, with and without edge-aware filtering.

Log-normal & Log-Poisson singularity spectra

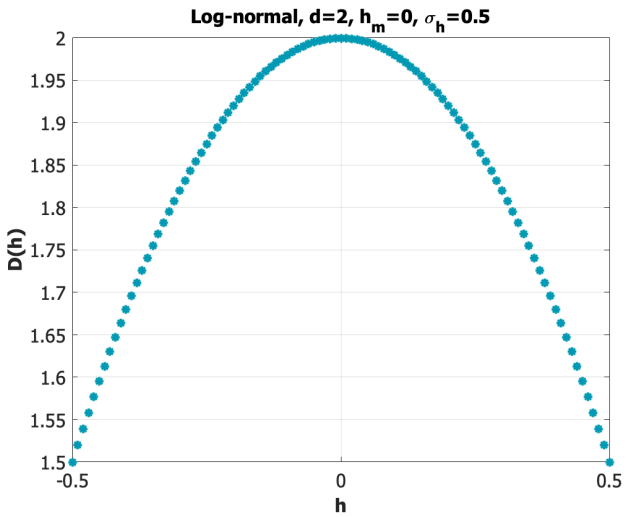

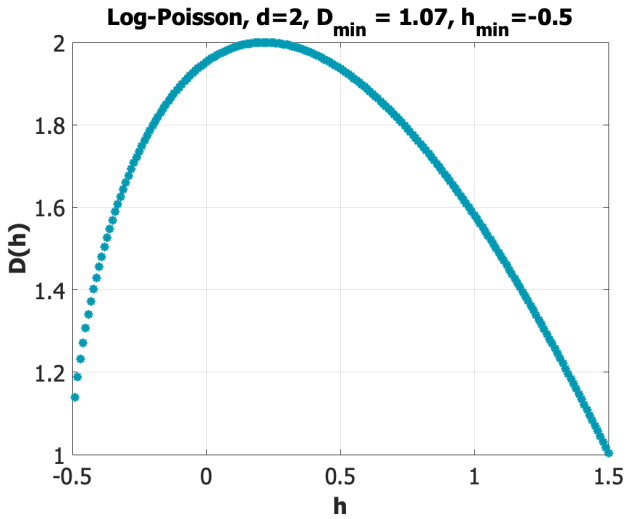

Log-normal parabolic spectrum in $\mathbb{R}^d$: $D(\mathbf{h}) = d - \frac{1}{2}\left(\frac{\mathbf{h}-\mathbf{h}_m}{\sigma_\mathbf{h}}\right)^2$.

Log-Poisson non-symmetric spectrum in $\mathbb{R}^d$:

$D(\mathbf{h}) = D_{\min} + (d - D_{\min})\omega(\mathbf{h})(1 - \log\omega(\mathbf{h}))$,

$\omega(\mathbf{h}) = \frac{\mathbf{h}-\mathbf{h}_{\min}}{(d-D_{\min})(-\log\beta)}$, β dissipation parameter $(0 < \beta < 1)$:

$\beta = 1 + \frac{\mathbf{h}_{\min}}{d - D_{\min}}$.

[Kolmogorov1962; VazquezSemadeni1994; She-Leveque1994; Gledzer1996]

5
Checking scale invariance
of a map

Counting-box like method

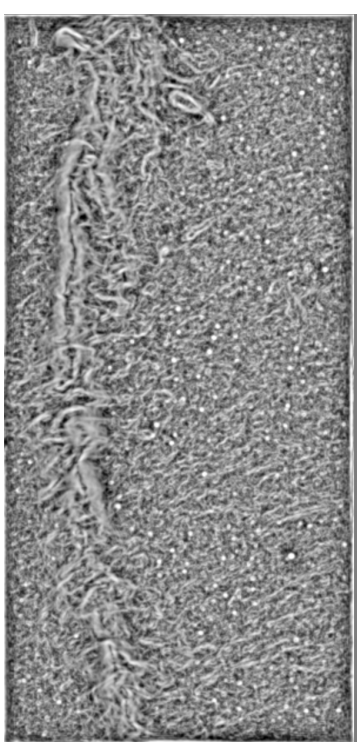

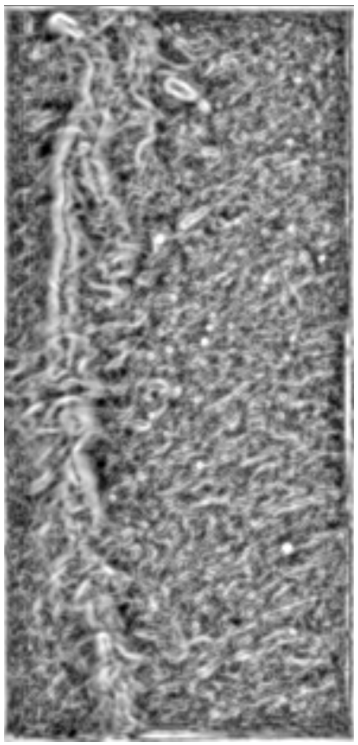

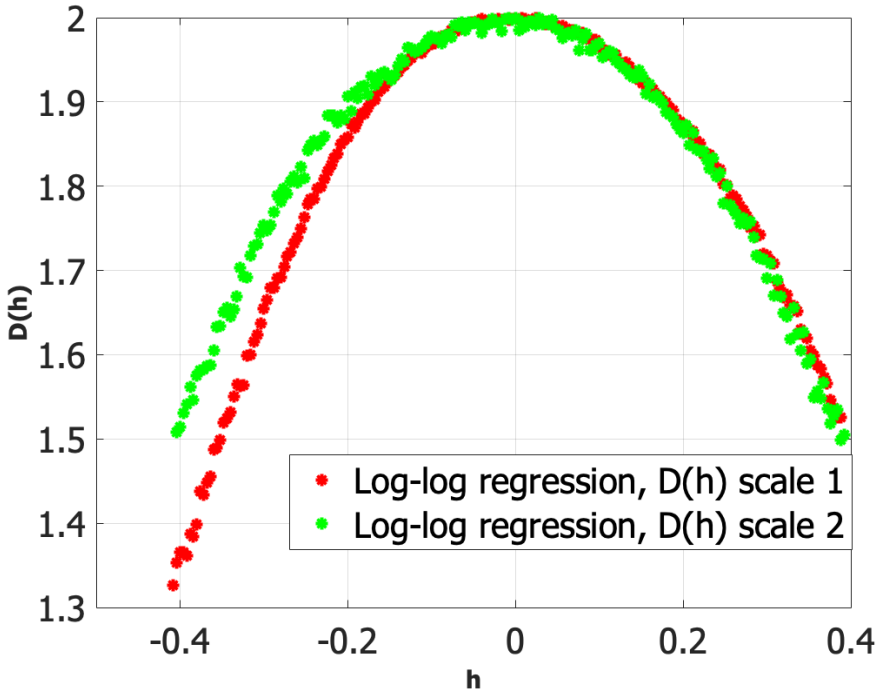

Enhanced counting box: gradient modulus wavelet projection method. Two consecutive scales.

Advanced microcanonical: correlation measure

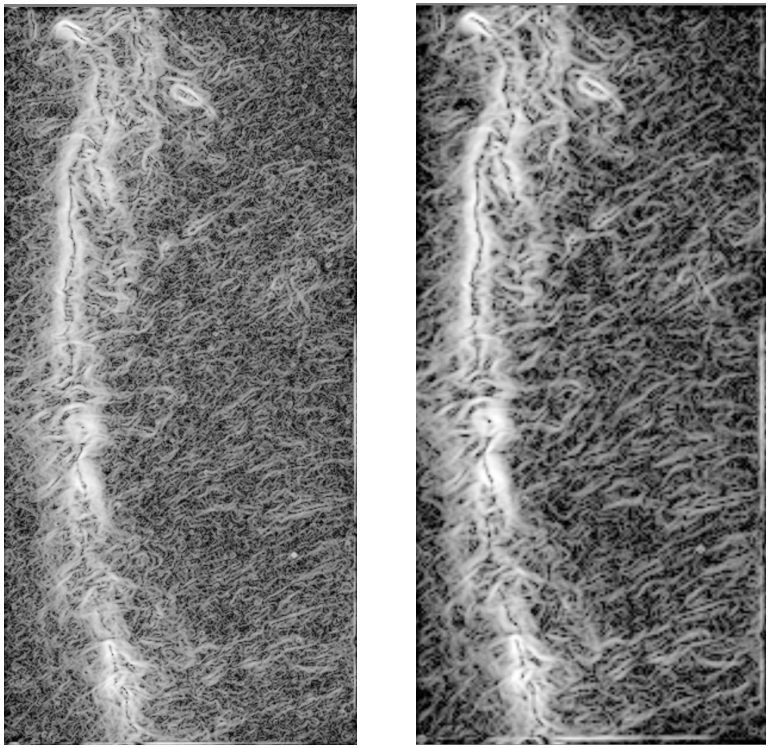

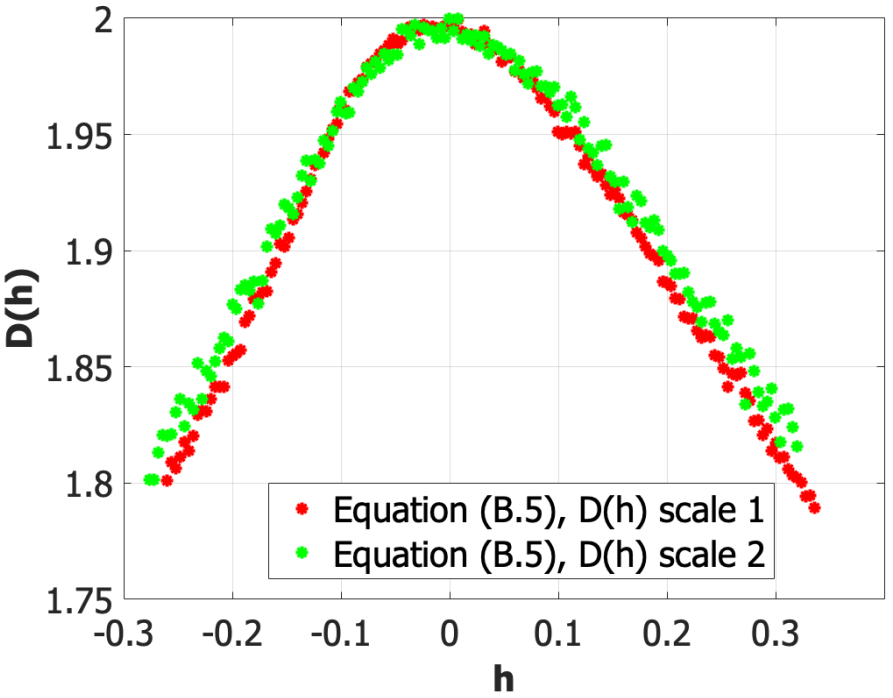

Correlation measure: scale invariance checked on two consecutive scales.

6
Structures function method:
inertial range of a turbulent field

2D structure function method

Inertial range determination.

MHD simulations determination through scaling of partition functions.
Musca $\rightarrow$ 2D structure functions,

If $\mathbf{x}_1$ and $\mathbf{x}_2$ are points in the 2D signal domain, the existence of scaling laws for a certain range of spatial distances is verified when

[Venugopal2006b; Renosh2015] $\langle |s(\mathbf{x}_1) - s(\mathbf{x}_2)|^q \rangle \sim \|\mathbf{x}_1 - \mathbf{x}_2\|^{\zeta(q)}$.

2D structure function method: Musca

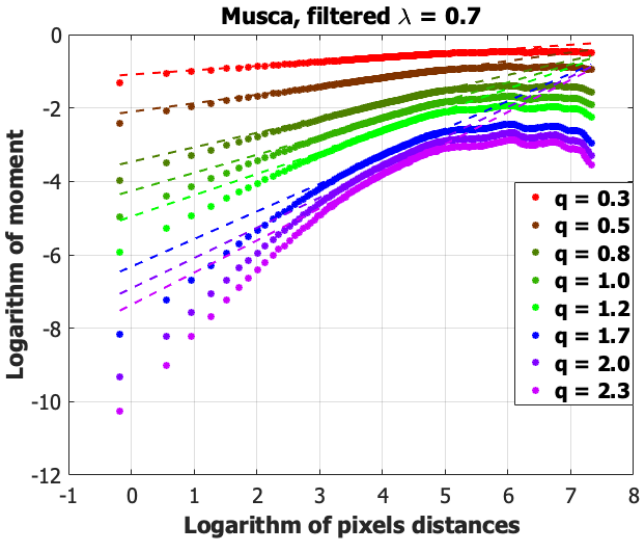

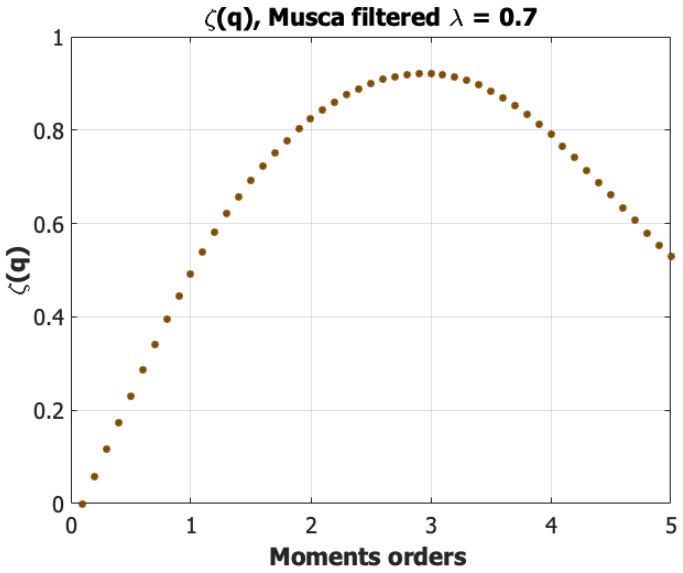

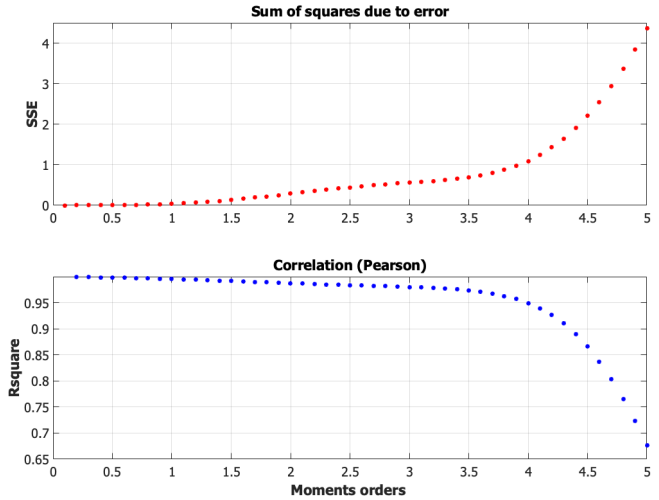

Inertial range corresponds to $\rightarrow [0.053, 0.65]$ pc. Middel panel: resulting map $q \mapsto \zeta(q)$. Right: quality decreases with the moment order q.

2D structure function method: MHD simulation

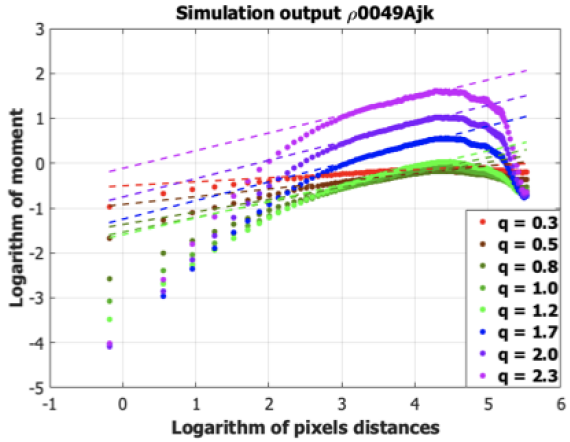

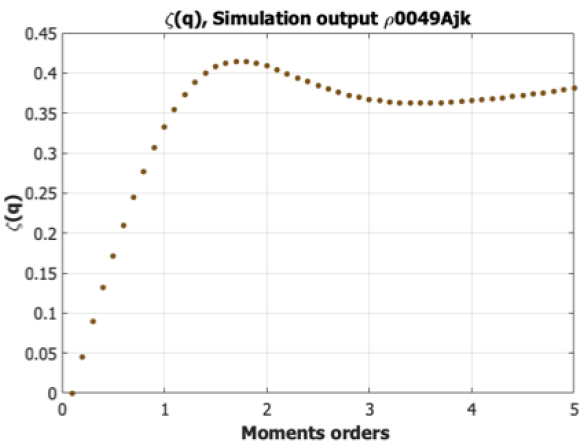

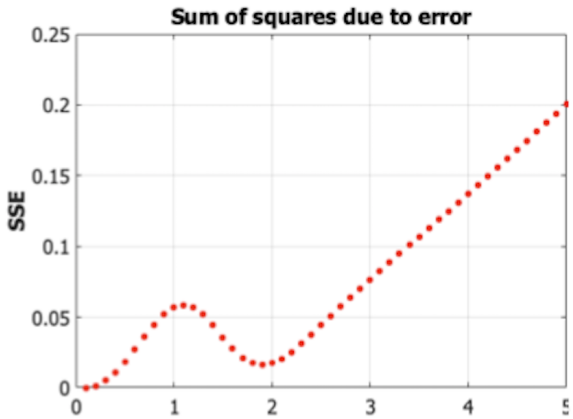

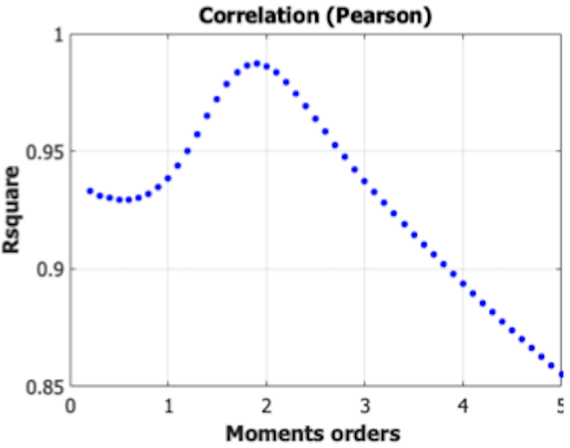

5×10^8 couples of points $(\mathbf{x}_1, \mathbf{x}_2)$ chosen uniformly ; moments q between 0.1 and 5.

7
Simulation data

MHD data

Ideal MHD equations are solved on a uniform 3D cubic grid using a total variation diminishing scheme (TVD).

[Stone1998; Truelove1998; Kim1999; Dib2007, 2008]

MHD data

Ideal MHD equations are solved on a uniform 3D cubic grid using a total variation diminishing scheme (TVD).

In order to achieve second-order accuracy in time, an updated step of the momentum density due to the gravitational force is implemented.

[Stone1998; Truelove1998; Kim1999; Dib2007, 2008]

MHD data

Ideal MHD equations are solved on a uniform 3D cubic grid using a total variation diminishing scheme (TVD).

In order to achieve second-order accuracy in time, an updated step of the momentum density due to the gravitational force is implemented.

Turbulence is continuously driven in the simulation box and the kinetic energy input rate is adjusted such as to maintain a constant specified *rms* sonic Mach number $M_s = 10$. Kinetic energy is injected at large scales, in the wave number range $k = 1 - 2$. When converted into physical units, the models correspond to a box size of 4 pc and an average number density of 500 cm^{-3}. The corresponding column density is thus $\sim 5\,10^{21}$ cm^{-2}, which is similar to that of many molecular clouds except for those associated with massive star formation.

[Stone1998; Truelove1998; Kim1999; Dib2007, 2008]

MHD data

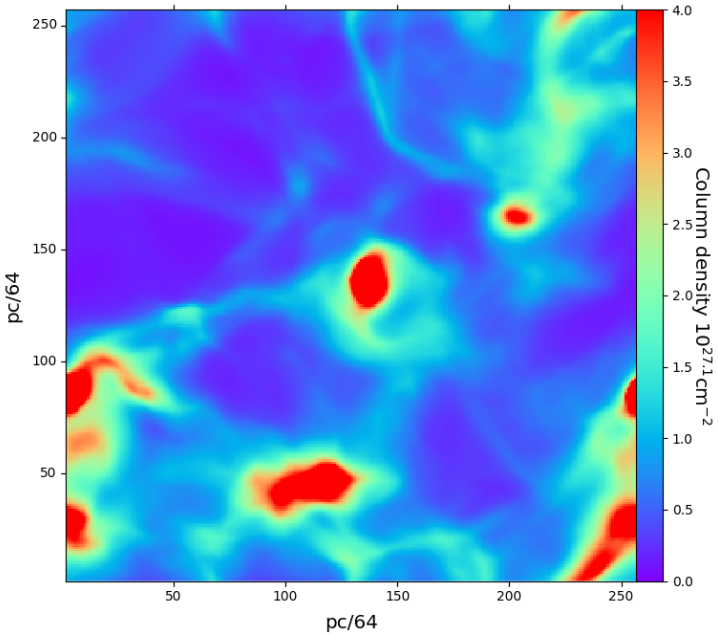

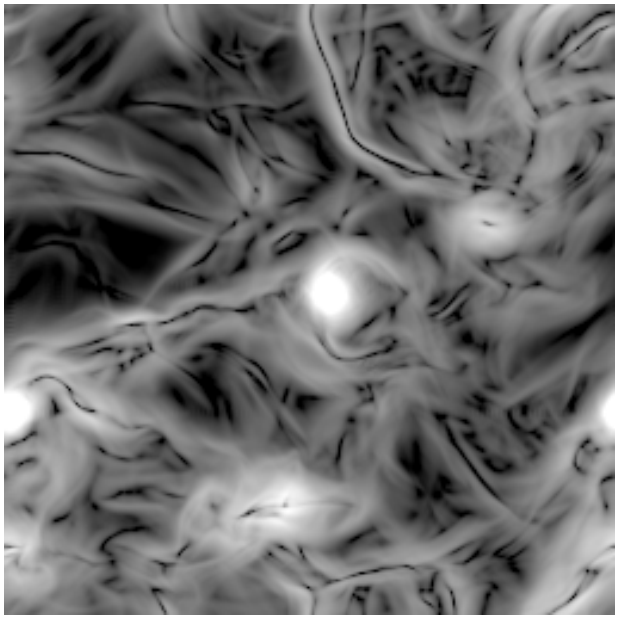

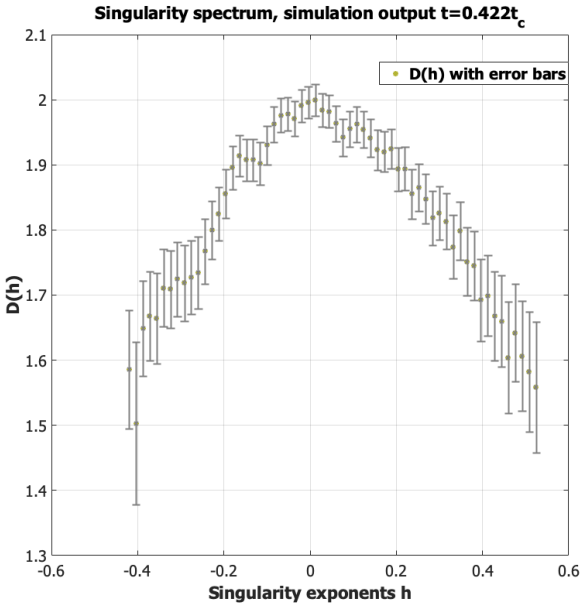

Left panel: output shown here corresponds to the hydrodynamical case with no magnetic field at time $t = 0.422\, t_c$.

MHD data

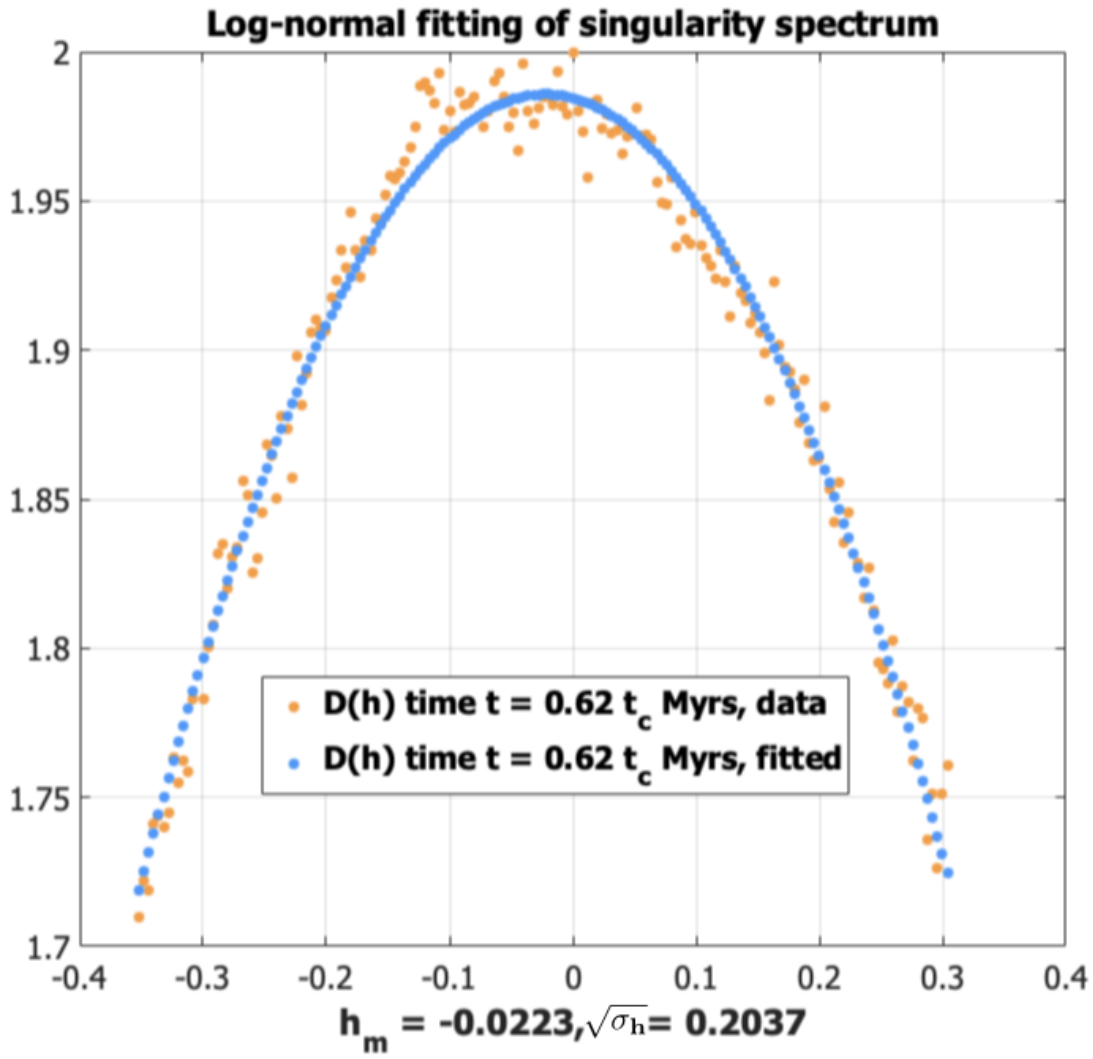
Log-normal fitting of singularity spectrum
2
1.95
1.9
1.85
1.8
1.75
1.7
-0.4
-0.3
-0.2
-0.1
0
0.1
0.2
0.3
0.4
D(h) time t = 0.62 t_c Myrs, data
D(h) time t = 0.62 t_c Myrs, fitted
h_m = -0.0223, √σ_h = 0.2037

8
Analysis of turbulent dynamics
of the Herschel Musca flux density map

Musca, full map. Deviation from log-normality

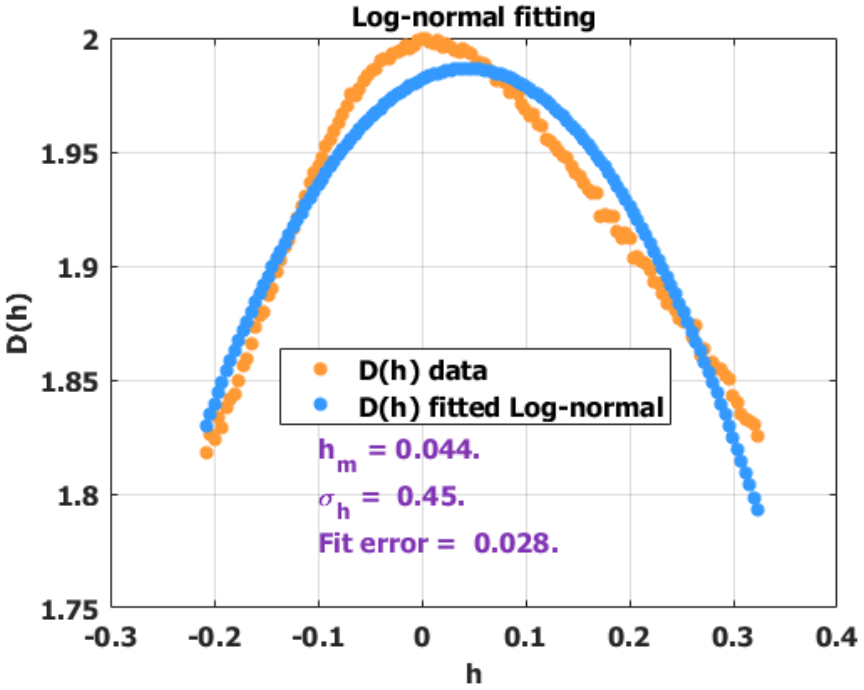

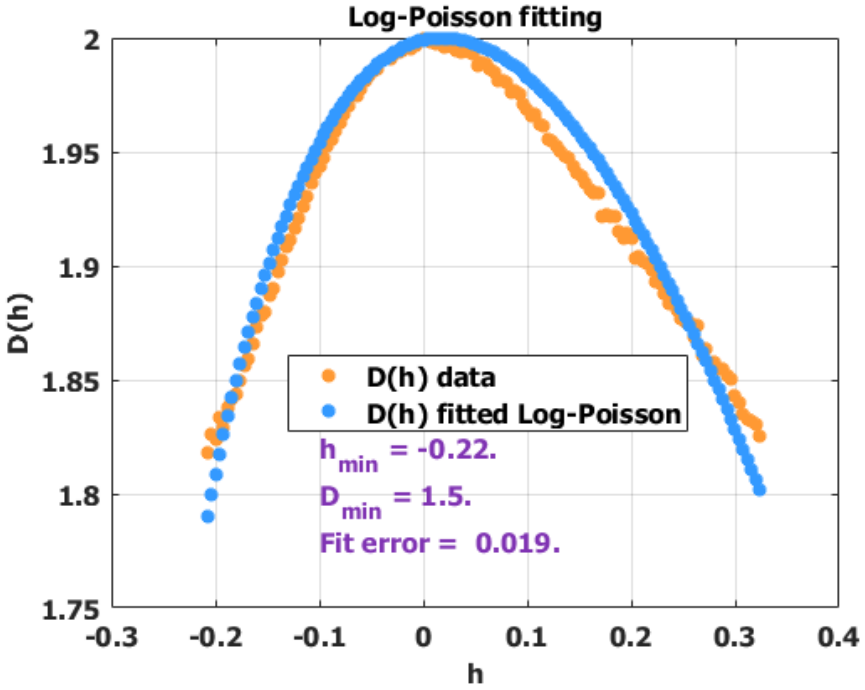

Left: the singularity spectrum of the filtered ($\lambda = 0.7$) Musca 250 μm observational map (in orange) is fitted against a log-normal parabolic spectrum (blue). Right: the singularity spectrum of the of the filtered ($\lambda = 0.7$) Musca 250 μm observational map (in orange) is fitted against a log-Poisson singularity spectrum (blue).

Musca Regions of Interest (ROIs)

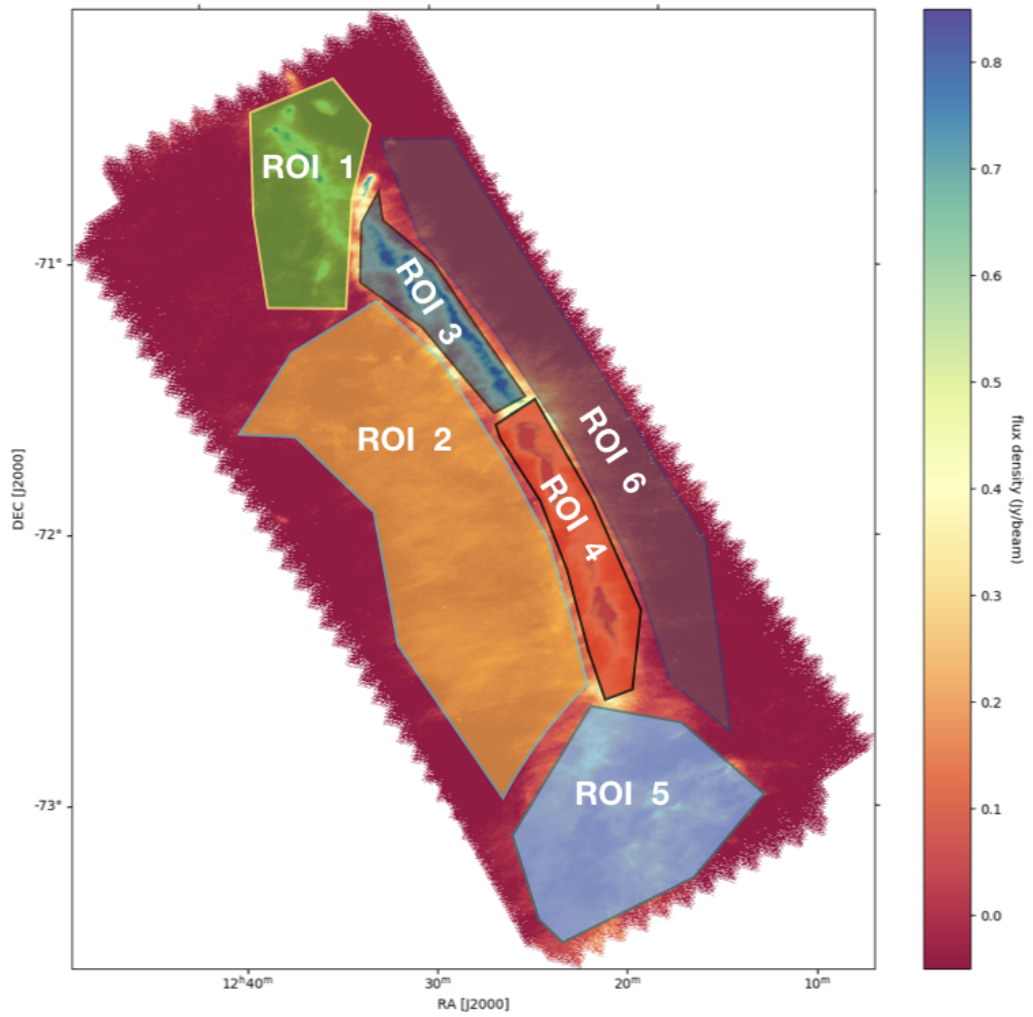

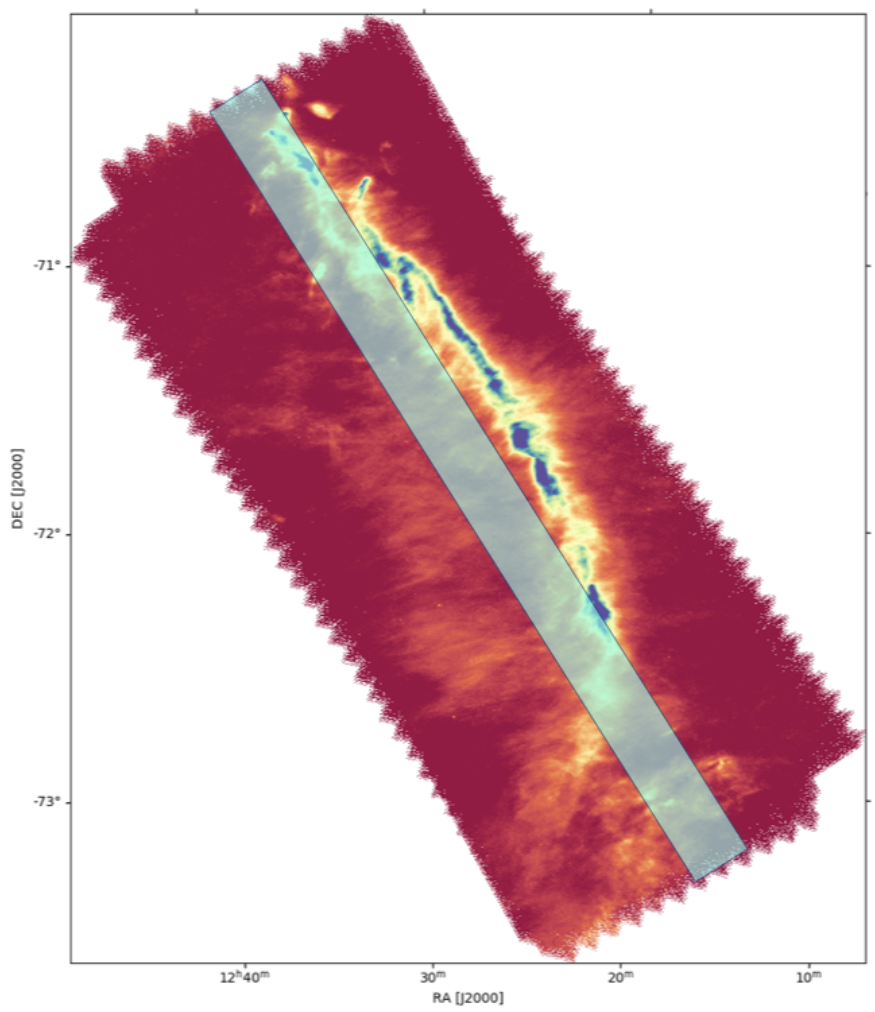

Musca: deviation from log-normality

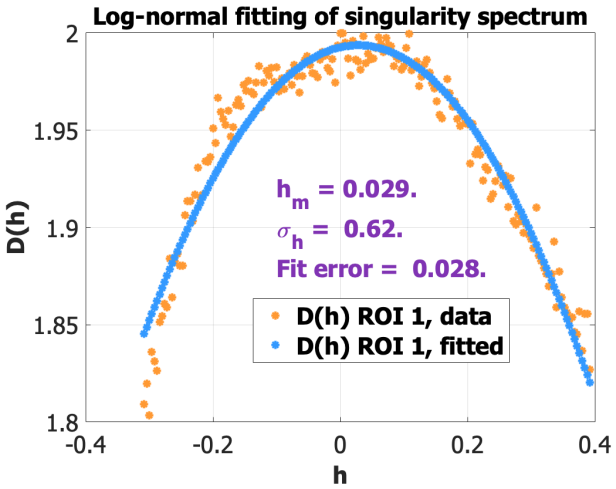

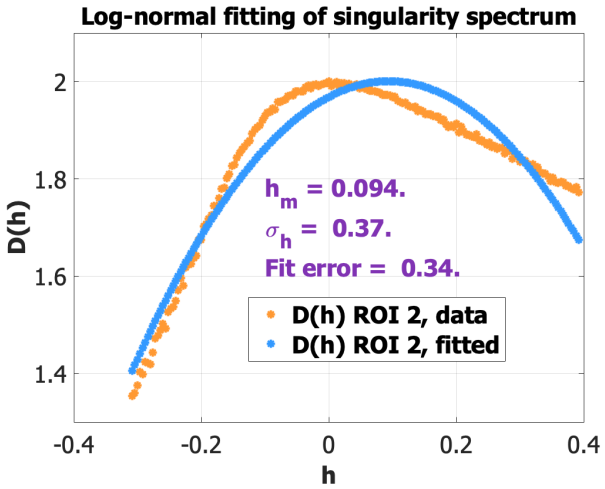

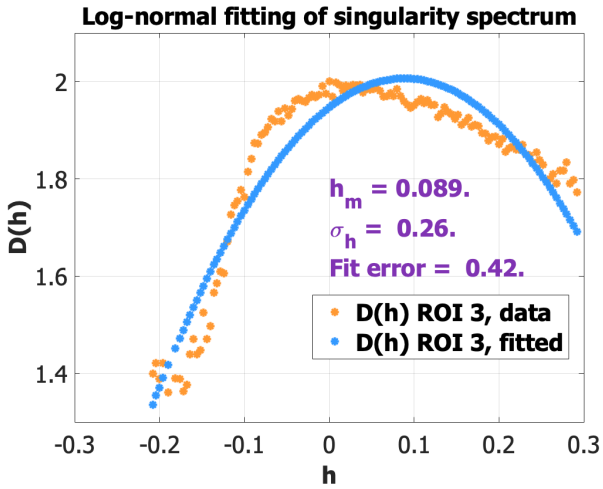

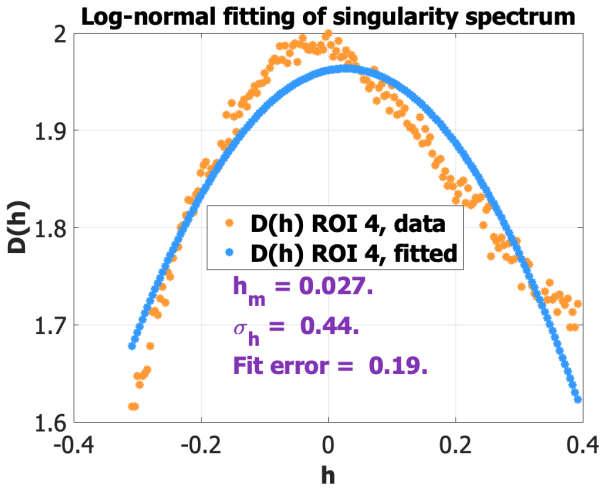

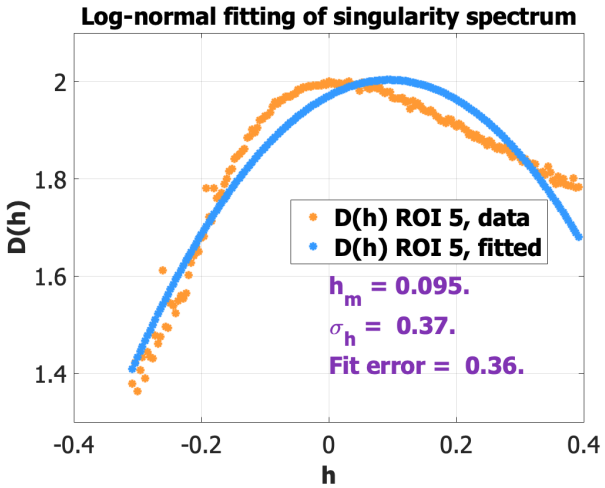

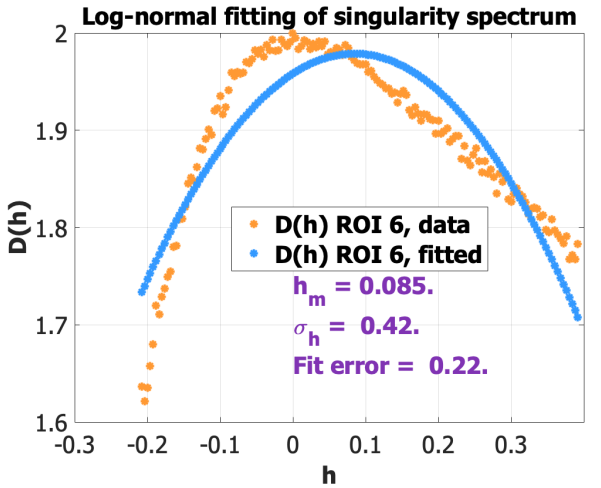

Musca: deviation from log-normality

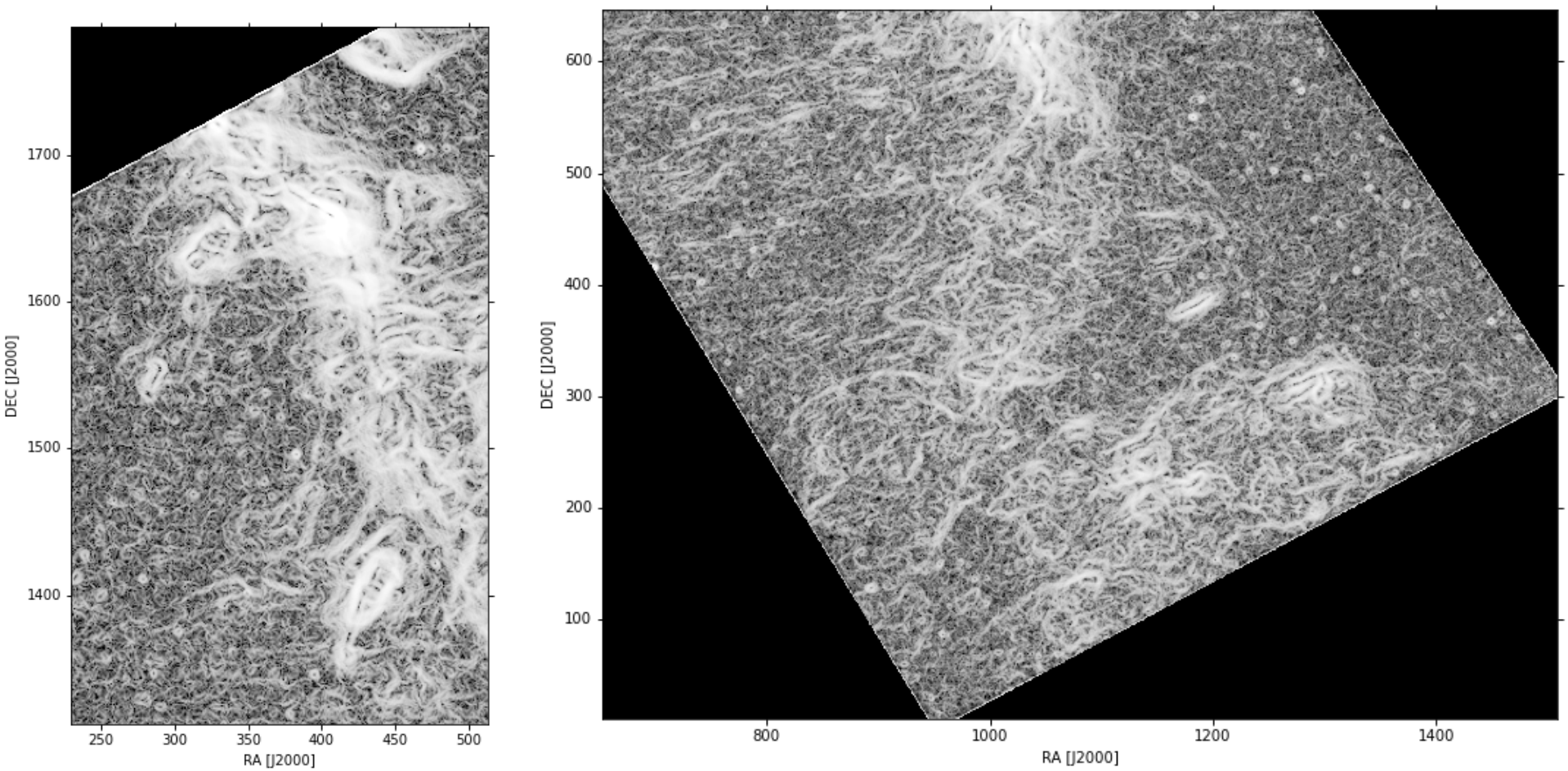

Distribution of the singularity exponents in ROI1 (left) and in the southern region of Musca ROI5 (right). Both regions show complex linear structures, but of different sizes and organisation.

Temporary conclusion

What causes deviation from log-normality ?

Temporary conclusion

What causes deviation from log-normality ?

Dynamic intermittency instead of spatial intermittency ?

Temporary conclusion

What causes deviation from log-normality ?

Dynamic intermittency instead of spatial intermittency ?

Implication on star formation ?

Temporary conclusion

What causes deviation from log-normality ?

Dynamic intermittency instead of spatial intermittency ?

Implication on star formation ?

To be continued...

9
Thank you.